Bioorganic Chemistry 153 (2024) 107895

Contents lists available at ScienceDirect

Bioorganic Chemistry

journal homepage: www.elsevier.com/locate/bioorg

Rivastigmine structure-based hybrids as potential multi-target anti-Alzheimer's drug candidates

Rosalba Leuci [a], Stefan Simic [b], Antonio Carrieri [a], Sílvia Chaves [c], Gabriella La Spada [a], Leonardo Brunetti [a], Paolo Tortorella [a], Fulvio Loiodice [a], Antonio Laghezza [a], Marco Catto [a], M.Amélia Santos [c], Vincenzo Tufarelli [d], Judith Wackerlig [b], Luca Piemontese [a,*]

[a] Department of Pharmacy—Pharmaceutical Sciences, University of Bari Aldo Moro, via E. Orabona 4, 70126 Bari, Italy
[b] Department of Pharmaceutical Sciences, Faculty of Life Sciences, University of Vienna, 1090 Vienna, Austria
[c] Centro de Química Estrutural, Departamento de Engenharia Química, Institute of Molecular Sciences, Instituto Superior Técnico, Universidade de Lisboa, Av. Rovisco Pais 1, Lisboa 1049-001, Portugal
[d] Department of Precision and Regenerative Medicine and Jonian Area (DiMePRe-J), Section of Veterinary Science and Animal Production, University of Bari Aldo Moro, Valenzano, 70010, Italy

ARTICLE INFO

Keywords:
Enzyme inhibitors
Alzheimer's disease
Rivastigmine mimetics
Multipotent drugs
ChEs
Chelating agents
Docking
MAOs
FAAH
Neurodegeneration
Pharmacokinetics
Cytotoxicity

ABSTRACT

In recent years, an increasing amount of work has been carried out regarding the study of the etiopathology of Alzheimer's Disease (AD). This neurodegenerative disease is characterized by several organic and molecular correlates, which paint a complex picture that also reflects the historic challenge faced by the worldwide scientific community in finding an effective cure for it.

In this paper, we describe the synthesis of novel rivastigmine derivatives and their characterization as wide-spectrum enzyme (AChE, BChE, FAAH, MAO-A and MAO-B) inhibitors with potential application in the therapy of AD following the paradigm of multi-target design. 5 (ROS151) and 23 show similar inhibitory profile compared to donepezil on cholinesterases, and ca. *two hundred twenty-three* and eighty-seven times more active than rivastigmine on AChE. Moreover, ROS151 was found to be a potential metal chelator. Compounds 6 and 8 are very interesting and original multi-functional promising hybrids, with comparable potency on distinct panels of enzymes. All these promising rivastigmine-like hybrids were assayed for their pharmacokinetic properties by using different bio-analytical techniques, showing interesting applicability profiles. Moreover, cytotoxicity assays displayed a safety profile on three different cell lines.

1. Introduction

Alzheimer's disease (AD) is the most common aging-related neurodegenerative disorder. It is characterized by a progressive loss of cognitive functions and represents a social and economic emergency [1,2]. Its etiopathology is still unknown, though several hypotheses have been formulated [3–6]. The worldwide recognized urgency for new effective treatments is evidenced by the enormous pipeline of drugs that have been explored along the time but, unfortunately, without effective disease-modifying effects. An important hallmark of AD is the progressive reduction in cholinergic transmission linked to lower concentrations of the neurotransmitter acetylcholine (ACh). Thus, the standard therapeutic strategy against AD is the inhibition of acetylcholinesterase (AChE), the most important catabolic enzyme of ACh [7].

AChE is found in high concentrations in red blood cells and in the nervous system, particularly at neuromuscular junctions and cholinergic brain synapses [8]. On the other hand, the enzyme butyrylcholinesterase (BChE, also known as pseudocholinesterase), is a non-specific type of cholinesterase enzyme that hydrolyzes different types of choline esters. BChE is ubiquitous, with particularly high concentrations in the human liver, blood serum, pancreas and central nervous system. In the brain, BChE is mainly expressed by glial and endothelial cells [9].

At low ACh concentrations, AChE is more efficient than BChE. However, at higher ACh concentrations, this relationship is reversed [9]. In the past, the importance of BChE was initially underestimated due to its lower expression in human brain compared to AChE [10]. However, recent studies have confirmed its key role in co-regulating ACh in the brains of patients diagnosed with neurodegenerative disorders such as

* Corresponding author.
E-mail address: luca.piemontese@uniba.it (L. Piemontese).

https://doi.org/10.1016/j.bioorg.2024.107895
Received 10 September 2024; Received in revised form 4 October 2024; Accepted 14 October 2024
Available online 18 October 2024

AD [10]. In fact, under these circumstances, AChE levels decrease up to 85 % in certain areas of the brain, while the concentration of BChE (in particular the G1 isoform) increases as the disease progresses, with the ratio BChE/AChE rising from 0.2 to 11.33 [11]. For this reason, the inhibition of both cholinesterases can improve the clinical efficacy of potential new drugs [12].

Cholinesterases (ChEs) are not the only proteins potentially involved in the etiopathogenesis of AD. Among catalytic enzymes, monoamine oxidase (MAO) mediates the oxidative deamination of amines, including many neurotransmitters. Its two isoforms, MAO-A and MAO-B, are similar in structure but different in tissue distribution and ligands [13,14]. Because the alteration in the concentration of neurotransmitters in the brain is usually connected with various neurological disorders, such as depression, AD and PD (Parkinson's disease), MAOs have become a target for their treatment [15]. In particular, selective MAO-A inhibitors are used as drugs for depression and anxiety disorders, while selective MAO-B inhibition is desirable for the treatment of AD and PD. In general, selective inhibition seems to reduce side effects [13].

The neurodegeneration in AD is also linked to the aggregation of β-amyloid protein (Aβ) in plaques and the formation of neurofibrillary tangles due to the hyperphosphorylation of *tau* protein. In particular, Aβ plaques cause an increase in inflammation and oxidative stress [3,5]. The dyshomeostasis of metals, in particular copper, zinc, and iron, is also associated with neurodegeneration, which makes chelating agents potential drugs for the treatment of AD [16–18].

Recently, the involvement of the endocannabinoid system (ECS) in the pathology has been studied and demonstrated [19]. In particular, AD patients show a significant reduction in the expression of the cannabinoid receptor 1 (CB1) in neurons located close to amyloid plaques, associated with overexpression of the CB2 receptor and Fatty Acid Amide Hydrolase (FAAH), the enzyme responsible for the metabolism of anandamide (AEA) and other endocannabinoids [19]. The pharmacological inhibition of FAAH has thus been proposed as a new target for the treatment of AD in order to reduce neuroinflammation [20].

Among currently approved anti-AD drugs it is possible to find three inhibitors of ChEs (donepezil, rivastigmine and galantamine) [21] and memantine, an antagonist of the glutamate receptor NMDA (*N*-methyl-d-aspartate) [22]. More recently, monoclonal antibodies, namely aducanumab, lecanemab and donanemab, targeting toxic Aβ oligomers have entered the market as the first disease-modifying therapeutics (DMTs) [23].

Currently available small molecule drugs act on single targets and they are only symptomatic, with no effect on the initiation and progression of AD [24]. Due to the probable multifactorial origin of AD, researchers have focused on the design of new multifunctional molecules, capable of acting simultaneously on several pharmacological targets [25]. Compared to the traditional therapeutic strategy based on the "one molecule – one target" principle, the new "multi-target directed ligand" (MTDL) approach is based on the "one molecule – multiple targets" paradigm and aims to develop agents with potentially higher therapeutic efficacy than traditional drugs [6,26].

This paradigm was followed in one of our recent works that reported the synthesis and biological evaluation of twenty hybrids containing a portion mimicking the current anti-AD drug donepezil (*N*-benzylpiperazine or *N*-benzylpiperidine), condensed via an amide bond with ten different aryloxyacetic acids [27]. Final compounds were tested on AChE, BChE and FAAH. Some of them demonstrated excellent activity against ChEs, with an IC_{50} higher than donepezil, whereas others had a better multi-target profile, even if the activity on FAAH was found in the micromolar range (not less than 16.9 μM and up to >100 μM) and these molecules can be considered only promising hit compounds, an important starting point for a new series [27]. The most potent compound of the series, **SON38** (Fig. 1a), was also able to chelate bivalent copper [27] and it has been candidate as a pharmacological tool.

Following the same MTDL approach, this work introduces new hybrids (**1**–**24**, Fig. 1b) of rivastigmine (another anti-AD drug) and aryloxyacetic acids, linked with an amide bond. In particular, taking inspiration from the previous results mentioned above [27], four aryloxyacetic acids were chosen: two of them presenting a nitro group in *ortho* position and a halogen (chlorine atom in position 4 or fluorine atom in position 5) for their activity on ChEs, one with a phenyl ring as *para*-substitution for the inhibition on FAAH, and one containing only chlorine atom in *para* position for the multi-target action.

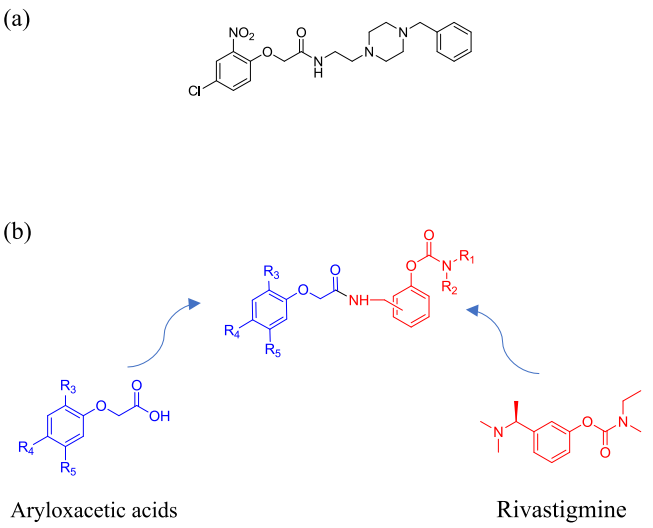

Fig. 1. (a) **SON38** [27]. (b) Drug design and general structure of hybrids **1**–**24**.

The advantage of present option for rivastigmine is due to its inhibitory capacity of both cholinesterases, while donepezil is a selective AChE inhibitor [27]. Moreover, differently from donepezil, rivastigmine is a pseudo-irreversible inhibitor, because its carbamate function binds the esterase site of cholinesterase for a longer time than the acetate moiety of its physiological substrate ACh [28]. For these reasons, this drug is widely used in therapy even though its potency towards AChE is lower than that of donepezil.

Additionally, our recent works reported further activity on MAOs, in particular MAO-A, for rivastigmine-like compounds [29]. Differently from these works [29,30], in this new series, the rivastigmine-like portion was varied on the position of carbamate group and the alkyl substituents on its nitrogen atom, searching for a different selectivity on this target. Twenty-four compounds were tested *in vitro* as inhibitors of a wider panel of enzymes comprising AChE, BChE, FAAH, MAO-A and MAO-B. Drug-likeness predictions were also performed, and some pharmacokinetic properties were evaluated through analytical methods and compared to the calculated ones. The same hybrids were evaluated for their cytotoxicity on three different cell lines. In addition, the kinetics of the most active compound on AChE, **5** or **ROS151**, has been evaluated with the aim to clarify the possible mechanism of action on this enzyme. Additionally, this hybrid was evaluated for its ability to chelate copper and iron cations, considering the suggestions of docking calculations and the similarities of the structure with other chelators [27].

2. Results

2.1. Chemistry

The synthesis of compounds **1**–**24** is described in Scheme 1. Intermediates **33a-35a** were prepared following previously reported procedures [27], starting from the appropriate commercial substituted phenols and ethyl bromoacetate, using sodium ethoxide as a base. The basic hydrolysis of **33a–35a** gave acids **33**–**35.**

The carbamates **25a–32a** were obtained by condensation of the suitable commercial carbamoyl chloride with the appropriate

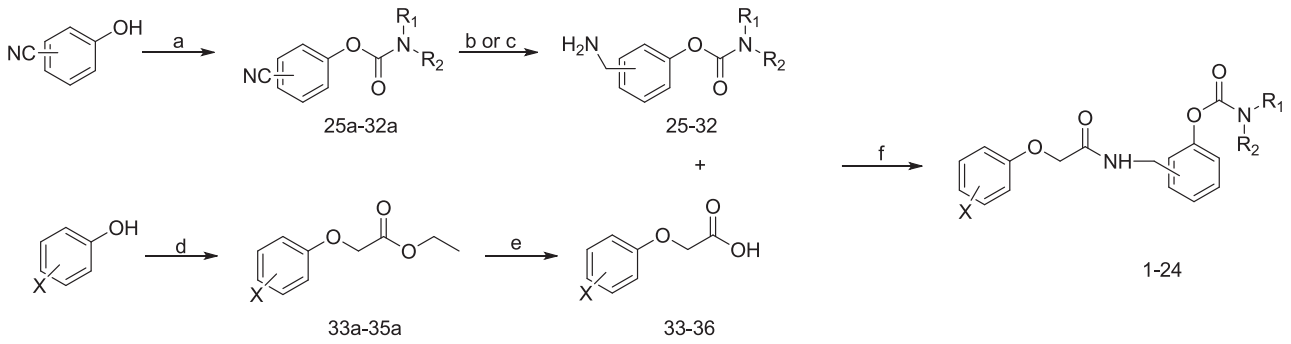

Scheme 1. (a) *N,N*-dialkylcarbamoyl chloride, TEA, reflux 5 h → RT overnight; (b) Pd/C 10 %, abs EtOH, H_2 2 atm, RT, overnight; (c) Pd/C 10 %, MeOH, H_2 4 atm, RT, 4 h; (d) Na, abs EtOH, ethyl bromoacetate, reflux, 24 h; e) 1 N NaOH, THF, RT, 5 h (f) HOBt, DIC, CH_2Cl_2, RT, overnight.

cyanophenol in triethylamine (TEA). The subsequent catalytic hydrogenation of cyano group of **25a-32a** using Pd/C 10 % as a catalyst afforded primary amines **25**–**32**.

Final compounds **1**–**24** were prepared by the condensation of acids **33**–**36** (**36** was commercially available) and the primary amines **25**–**32** by using of 1-hydroxybenzotriazole hydrate (HOBt) and *N,N*′-diisopropylcarbodiimide (DIC) as condensing agents.

2.2. Biological assays

As previously mentioned, in this work, the substituents of the phenoxy group of compounds **1**–**24** were selected based on previous studies [27] and supported by preliminary docking evaluation. The capability of these molecules to inhibit the human enzymes AChE, BChE, FAAH, MAO-A and MAO-B is reported in Table 1 as percentage of inhibition at a fixed ligand concentration (10 μM) or as IC_{50} (μM) for compounds

Table 1

Biological activities of compounds **1**–**24** towards AChE, BChE, FAAH, MAO-A and MAO-B.

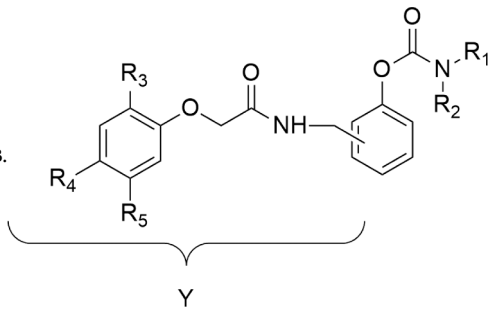

							IC_{50}, μM[a]				
Cpd	Y*	R_1	R_2	R_3	R_4	R_5	*h*AChE	*eq*BChE	*h*FAAH	*h*MAO-A	*h*MAO-B
1	*ortho*	Et	Et	NO_2	H	F	3.00 ± 0.72	39 ± 3 %[b]	39.7 ± 9.36[a]	11 ± 5 %[b]	56 ± 5 %[b]
2	*ortho*	Et	Me	NO_2	H	F	2.11 ± 0.16	61 ± 5 %[b]	8.09 ± 1.71[a]	43 ± 1 %[b]	4.52 ± 1.06
3	*para*	Et	Et	NO_2	H	F	4.33 ± 0.19	49 ± 2 %[b]	n.a.	21 ± 5 %[b]	1.91 ± 0.98
4	*meta*	Et	Et	NO_2	H	F	4.95 ± 0.98	62 ± 1 %[b]	30.0 ± 10.1[a]	23 ± 5 %[b]	55 ± 1 %[b]
5	*meta*	Me	Me	NO_2	H	F	0.014 ± 0.006	1.68 ± 0.40	8.17 ± 3.77[a]	n.a.	41 ± 8 %[b]
6	*meta*	Et	Me	NO_2	H	F	6.59 ± 1.63	60 ± 2 %[b]	6.29 ± 3.31[a]	7 ± 5 %[b]	5.98 ± 1.64
7	*ortho*	Et	Et	H	Ph	H	4.83 ± 0.02	61 ± 3 %[b]	15.3 ± 1.76[a]	36 ± 3 %[b]	9.44 ± 1.19
8	*ortho*	Et	Me	H	Ph	H	32 ± 1 %[b]	1.69 ± 0.35	1.40 ± 0.25[a]	48 ± 3 %[b]	1.71 ± 0.75
9	*para*	Et	Et	H	Ph	H	5.13 ± 0.79	17 ± 5 %[b]	22.8 ± 6.93[a]	34 ± 3 %[b]	43 ± 4 %[b]
10	*meta*	Et	Et	H	Ph	H	50 ± 5 %[b]	5.36 ± 0.26	11.7 ± 0.98[a]	54 ± 5 %[b]	56 ± 1 %[b]
11	*meta*	Me	Me	H	Ph	H	52 ± 9 %[b]	53 ± 3 %[b]	10.7 ± 7.20[a]	n.a.	32 ± 4 %[b]
12	*meta*	Et	Me	H	Ph	H	39 ± 9 %[b]	60 ± 1 %[b]	14.3 ± 4.96[a]	n.a.	6.86 ± 0.90
13	*ortho*	Et	Me	H	Cl	H	33 ± 4 %[b]	54 ± 1 %[b]	6.93 ± 0.17[a]	35 ± 5 %[b]	13 ± 4 %[b]
14	*para*	Et	Et	H	Cl	H	4.80 ± 0.41	28 ± 2 %[b]	17.2 ± 5.77[a]	30 ± 3 %[b]	52 ± 3 %[b]
15	*para*	Me	Me	H	Cl	H	4.26 ± 0.45	59 ± 2 %[b]	15.9 ± 2.73[a]	13 ± 4 %[b]	38 ± 5 %[b]
16	*para*	Et	Me	H	Cl	H	4.44 ± 0.86	57 ± 1 %[b]	21.5 ± 0.44[a]	17 ± 5 %[b]	20 ± 5 %[b]
17	*meta*	Me	Me	H	Cl	H	45 ± 5 %[b]	52 ± 1 %[b]	3.35 ± 0.24[a]	n.a.	49 ± 8 %[b]
18	*meta*	Et	Me	H	Cl	H	40 ± 4 %[b]	33 ± 1 %[b]	9.93 ± 8.12[a]	27 ± 16 %[b]	36 ± 9 %[b]
19	*ortho*	Et	Me	NO_2	Cl	H	4.76 ± 0.51	46 ± 5 %[b]	14.2 ± 0.49[a]	n.a.	21 ± 8 %[b]
20	*para*	Et	Et	NO_2	Cl	H	2.86 ± 0.13	50 ± 3 %[b]	39.8 ± 6.54[a]	49 ± 3 %[b]	2.93 ± 0.39
21	*para*	Me	Me	NO_2	Cl	H	1.56 ± 0.37	2.11 ± 0.49	20.2 ± 6.65[a]	41 ± 3 %[b]	52 ± 5 %[b]
22	*para*	Et	Me	NO_2	Cl	H	55 ± 4 %[b]	59 ± 2 %[b]	32.2 ± 8.37[a]	44 ± 5 %[b]	2.47 ± 0.10
23	*meta*	Me	Me	NO_2	Cl	H	0.036 ± 0.007	2.76 ± 0.43	3.56 ± 0.09[a]	6 ± 5 %[b]	35 ± 3 %[b]
24	*meta*	Et	Me	NO_2	Cl	H	51 ± 2 %[b]	45 ± 1 %[b]	5.80 ± 2.69[a]	n.a.	6.66 ± 1.05
Donepezil							0.016 ± 0.002	2.31 ± 0.12	n.d.	n.d.	n.d.
Rivastigmine							3.12 ± 0.46	0.38 ± 0.02[c]	n.d.	n.d.	n.d.
JZL195							n.d.	n.d.	0.019 ± 0.003	n.d.	n.d.
Safinamide							n.d.	n.d.	n.d.	18 ± 3 %[b]	0.029 ± 0.001

*Position of carbamate group ([a]) Values are mean ± SEM (n = 3); ([b]) % inhibition at 10 μM; ([c]) assayed on *h*BChE; n.a. = not active, n.d. = not determined.

displaying inhibition >70 % at 10 μM for ChEs and MAOs, or >50 % at 50 μM for FAAH. Donepezil and rivastigmine were used as reference compounds for ChEs, while JZL195 and safinamide as reference compounds for FAAH and MAOs, respectively.

All compounds of the series are active against AChE. In particular, the presence of nitro group in *ortho* position of phenoxy ring and a halogen results in markedly enhanced activity (**1**–**6** and **19**–**24**), confirming data from the previously reported donepezil-like series [27]. Among them, hybrids **5** and **23**, presenting the carbamate moiety in *meta* position and dimethyl substitution, have comparable activity to reference compound donepezil (IC_{50} values of 0.014 μM and 0.036 μM, respectively *vs* IC_{50} = 0.016 μM of donepezil). Compounds lacking the nitro group in the aryloxy portion (**7**–**18**) have generally lower activities; moreover, ethyl-methyl substitution on the carbamic nitrogen seems to reduce compound potency.

In order to understand the inhibition mechanism of these compounds on AChE, a kinetic study was performed using the most potent and promising derivative **5** (**ROS 151**). It is well known that rivastigmine and other carbamates act through a pseudo-irreversible inhibition mechanism by forming a covalent bond with the serine at the catalytic site [31]. Indeed, our results revealed a non-competitive inhibition exerted by **ROS151** (Fig. 2), typical of dual binding site inhibitors installing interactions with both the peripheral and the catalytic binding sites of AChE, with $K_i = 43 \pm 6$ nM. We measured an IC_{50} value of 48 nM with a short (5 min) incubation time, actually higher than that obtained under standard conditions (IC_{50} = 14 nM), thus suggesting a partial irreversibility or at least a stabilization of binding at the catalytic site.

Inhibitory activity towards BChE is significant but generally lower than against AChE, with no relevant influence of the variations on rivastigmine-like portion and on phenoxy ring. For these reasons it is not easy to rationalize the data and consequently identify a SAR. Compounds **5**, **8**, **21** and **23** show the best results (IC_{50} values in the range 1.68–2.76 μM). Interestingly, among them, **21** has a very similar activity towards both ChEs, such as rivastigmine itself.

For FAAH inhibition, all compounds of the series, except **3**, are active, with a relatively small range of IC_{50} values, probably due to the distance of the chemical modifications from the pharmacophoric moiety. Overall, best compounds bear biphenyl and *para*-chlorine in aryloxy portion, in particular **8** (IC_{50} = 1.40 μM), containing the biphenyl group or the ethyl-methyl *ortho* carbamate, has the highest inhibitory activity on FAAH. Remarkably, these rivastigmine-based hybrids show potencies up to an order of magnitude higher than those of the previous donepezil-like hybrids [27].

MAOs were investigated as additional targets. In general, these hybrids are selective for MAO-B, with no or little activity at the tested concentration of 10 μM for MAO-A. This is in contrast with other recently developed rivastigmine derivatives which demonstrated a higher activity on MAO-A [29]. Although MAO-A is considered a target for the treatment of some neurological diseases, this selectivity towards MAO-B is preferable for the reduction of side effects in the potential treatment of dementia such as AD [13]. The best compounds on MAO-B are **3**, **8**, **20** and **22**, having their IC_{50} values in low micromolar range. Interestingly, dimethyl substitution of the carbamic function seems to be the worst one for the activity on this target, regardless of the substituted phenoxy moiety and the position of carbamate.

Crucially, one of the primary goals in the design of these hybrids was to find a good multi-target compound, whose IC_{50} values towards all selected targets would be in a similar range. Most compounds of the series are very promising from this point of view: they are active on at least three of the four tested targets (AChE, BChE, FAAH, MAO-B) and selective against MAO-A, with **6** and **8** as the best multi-target ones. These results are an important achievement, considering the higher activity compared to the hit compounds selected as multi-target in the previous series on FAAH [27]: this led to obtaining, for some hybrids, very similar inhibition values on a good number of targets.

In particular, compound **6** has approximately the same potency (IC_{50} values between 5.98 and 6.59 μM) towards three enzymes, namely AChE, FAAH and MAO-B, with a comparable activity on BChE (60 % at 10 μM).

On the other hand, compound **8**, has lower IC_{50} values towards BChE, FAAH and MAO-B within a relatively small range (1.40–1.71 μM); in this case, the absence of the nitro group in *ortho* position of the aryloxy nucleus, compared to the structure of **6**, markedly reduced its activity on AChE, confirming the key role of the substituent in the search of selective inhibitors on this specific target [27].

2.3. Pharmacokinetic properties

Biomimetic chromatography with high performance liquid chromatography (HPLC) methods were applied for the study of the pharmacokinetics of the most interesting compounds. The stationary phases selected were based on phospholipids and proteins, with the aim of mimicking biological settings. This enabled rather precise determination of certain ADME (absorption, distribution, metabolism and excretion) properties such as lipophilicity, plasma protein binding (PPB) on human serum albumin (HSA) and alpha-1 glycoprotein (AGP) and blood–brain barrier penetration [32,33].

According to Lipinski's rule of five, Log*P* should be less than 5 for

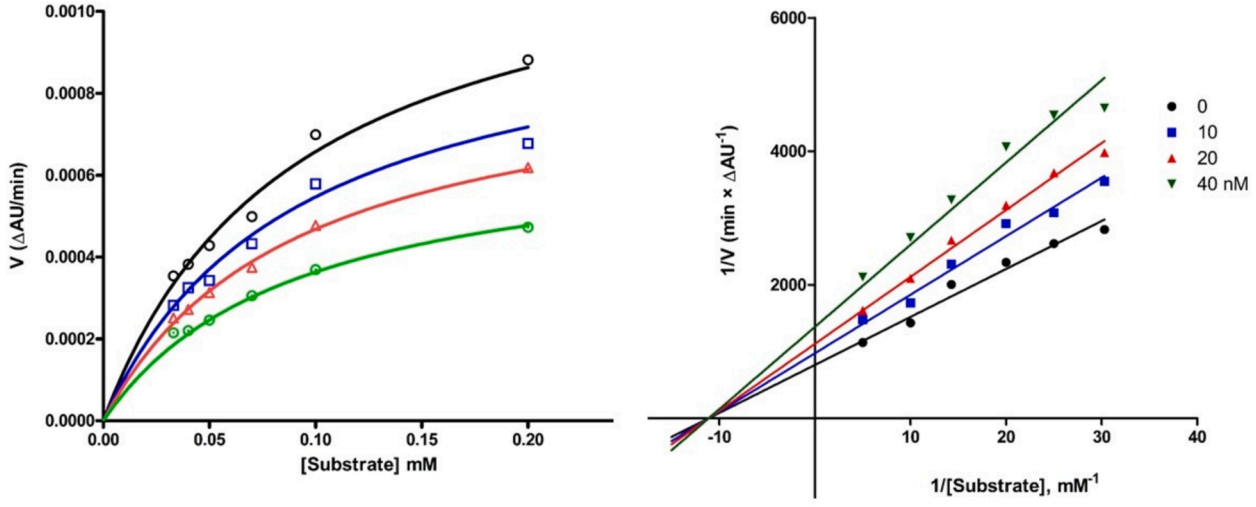

Fig. 2. Michaelis-Menten (left) and Lineweaver-Burk (right) plots of hAChE inhibition by ROS151.

optimal drug-likeness. An adapted version of this rule determines that the ideal value for the BBB penetration probability *via* passive diffusion is in the range from 2.0 to 3.5 [34]. Log*P* values for the four compounds of interest were found to be between 1.87 ± 0.20 and 3.83 ± 0.15 (see Table 2) all being well below 5 and in the suggested range, except **ROS151** being slightly lower and compound **8** being slightly higher than the lower and upper limit, respectively. Considering the experimental range these values are acceptable. The experimental values are also in line with the *in silico* prediction using the ACD/Chemsketch software (±12 %). Predicted values for Log*P* of rivastigmine and donepezil are 2.14 and 4.71, respectively. The optimized compounds are suggested to exhibit superior BBB penetration *via* passive diffusion compared to donepezil and similar to rivastigmine.

The four most biologically active compounds exhibit high $\%PPB_{HSA}$ in a range between 80 % and 89 % as shown in Table 3. In comparison, rivastigmine exhibits moderate PPB (below 79 %), while donepezil belongs to the drugs with high PPB as the four tested compounds. [35,36]. All compounds exhibit %PPB below 95 % being beneficial for drug safety [37]. They showed high affinity binding to both the human serum albumin and alpha-1 glycoprotein with values between 84 and 91 %, suggesting that the compounds are behaving more similarly to donepezil than to rivastigmine. From a therapeutic point of view the study of PPB can give insight into the potential bioavailability of a given compound, which must be assessed in the early stages of drug discovery. Further evaluation of the compounds regarding the behavior in the liver could provide even more insight regarding pharmacokinetics.

The four compounds possess coefficient of membrane permeability (P_m) values higher than 1.88 (between 2.8 and 11.2) and are therefore likely to exhibit positive blood–brain penetration. This is also acknowledging the passive diffusion passing of the blood brain barrier, as the Log*P* values are in the range of the probable BBB penetration (Table S1, see SI).

In vivo performance of drugs is influenced by their plasma stability which should be as high as possible. Plasma stability is essential in keeping an optimal half-life of the drug and acceptable drug concentration to achieve wanted pharmacological effect [32]. The compounds show high stability in human plasma (Table S2) with a percentage of unmetabolized compound between 88 and 93 % after 24 h of incubation at 37 °C (see SI). Plasma stability in rat plasma (Table S3, see SI) is similar to human plasma in the first four hours. After 24 h, decreased stability in rat plasma is observed (64 to 90 % unmetabolized compound) most likely due to differences in the enzymes of the species [36]. This comparison is very important for the development of future studies, considering that the next step could be the administration of the potential drug *in vivo*.

2.4. Cytotoxicity assays

The cytotoxicity of the four most promising hybrids (**5 – ROS151**, **6**, **8** and **23**) was evaluated via MTT assay on human tumor cells HepG2 (liver), MCF-7 (breast), and HEK-293 (kidney) which were incubated with the different compounds for 48 h (see Fig. 3).

Compounds did not show significant cytotoxic effects until a tested concentration of 30 μM.

Table 2
Experimental Log*P* evaluation with the RP-HPLC method (calculated with equation S1.; n = 3, CV* [%]) and *in silico* Log*P* determination with the ACD/ChemSketch software.

Compound	Log*P* + CV* [%]	ACD/ChemSketch Log*P*
23	2.29 ± 0.52	2.53
8	3.83 ± 0.15	4.34
6	2.33 ± 0.22	2.18
ROS151	1.87 ± 0.20	1.65

* coefficient of variation

Table 3
Results for PPB and P_m from the biomimetic chromatography assays; n = 3, CV* [%].

Compound	$\%PPB_{HSA}$	%HSA	%AGP	P_m + CV* [%]
23	88.5	88.2	89.9	6.19 ± 2.0
8	89.3	91.0	89.6	11.2 ± 0.6
6	83.3	85.7	90.6	4.29 ± 2.1
ROS151	79.7	83.7	90.0	2.81 ± 2.8
Rivastigmine	64.4	54.2	37.8	
Donepezil	85.2	82.3	73.6	

$\%PPB_{HSA}$. – calculated experimental total plasma protein binding measured on CHIRALPAK-HSA column (equation S2).
%HSA – estimated percent of binding to human serum albumin measured on CHIRALPAK-HSA column (equation S3).
%AGP – estimated percent of binding to alpha-1 glycoprotein measured on CHIRALPAK-AGP column (equation S4).
Pm – coefficient of membrane permeability (equation 1) measured on IAM.PC. DD.2 column.
* coefficient of variation.

2.5. Molecular docking calculation

Based on a wealth of experimental evidence gathered from X-ray crystallographic data, insights into the spatial arrangement of binders within the catalytic sites of their respective targets have been obtained. The superior activity of the most promising compounds was explained *via* molecular docking. Comparing binding poses with well-established potent inhibitors of esterases, amidases, and oxidases provided us *in silico* guidance and directives for evaluating assay data *in vitro*.

The binding sites of esterases are well-known and generally include a catalytic triad (Ser203, Glu334, and His447 in hAChE numbering), as well as catalytic CAS (Trp86 and Phe338), and peripheral PAS (Tyr72, Tyr124, and Trp286) anionic sites. These can be seen as anchoring points where ligands interact favourably with the enzyme, as evidenced by observations of X-ray complexes of hAChE [38] and hBChE [39] with established potent inhibitors.

As illustrated in Fig. 4, the most potent compound **ROS151** on hAChE occupies the enzyme entrance cavity extending towards the catalytic triad (CT) and instigates a diverse array of ligand–protein interactions, resembling those commonly observed in the molecular recognition systems of this enzyme. Notably, NHCO-substituted phenyl ring retrieves *edge-to-face* π-π stacking with Tyr337 and Tyr341 and it aids the establishing connections with the target surface, while the two methyl groups of the carbamate retrieve Van der Waals contacts with Trp86 and the same Tyr337. The central amide moiety plays a crucial role by producing an intramolecular hydrogen bond with the nitro substituent that is then capable to anchor the inhibitor's molecular scaffold, making additional hydrogen bonds with the backbone skeleton of Phe295 and Arg296. Moreover, the terminal phenoxy moiety contributes to additional stabilization participating in *face-to-face* π-π stacking interactions with Trp286.

This binding pattern, as demonstrated previously [27], could be considered a recurring chemical motif associated with the excellent activity of compounds featuring a nitro group and a halogen atom in the ortho and meta positions of the ring (e.g., compounds **1**–**6** and **19**–**24**).

It should be noted that the described interaction pattern may represent the initial mode of interaction for these hybrid compounds. Considering the presence of the rivastigmine-like fragment, it is plausible that these compounds undergo a conformational rearrangement, ultimately leading to covalent inhibition of the enzyme. This inhibition mechanism could involve acylation of the catalytic serine residue within the active site supporting the hypothesis suggested by the kinetic studies reported above.

Subsequently, one of the most potent compounds on eqBChE, **8**, was investigated but in this case, the precise replication of previously discussed binding poses was hindered by differences in the amino acid

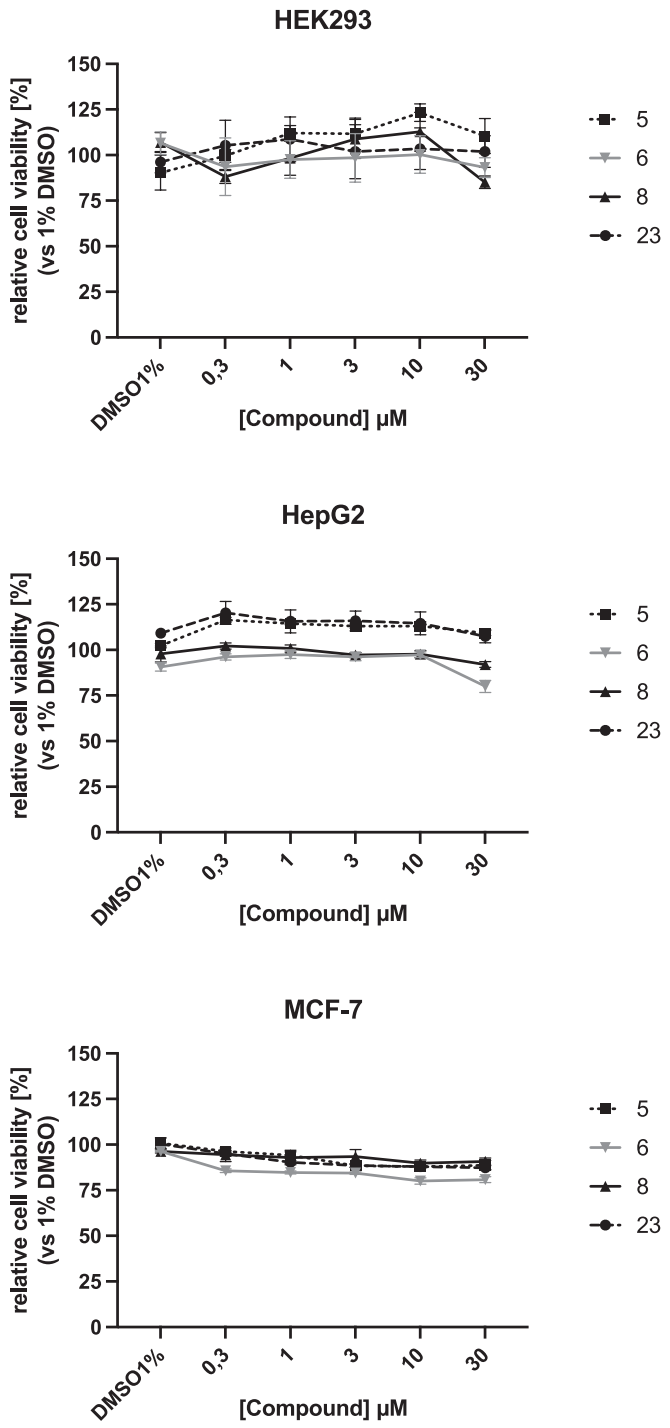

Fig. 3. Cell vitality measured by MTT assay. Compounds 5 (**ROS151**), 6, 8 and 23 possessed no cytotoxicity in HepG2, HEK293 and MCF-7 cells up to 30 µM (mean ± SEM of 3 independent experiment, n = 4).

composition of the CT, CAS, and PAS, as well as variations in the accessible surface of the active sites. Instead, a more bent conformation was observed, closely resembling the crystallographic structure of the human enzyme (eqBChE is not available in literature, but it is comparable to hBChE in terms of structure and for the estimation of inhibition activities, as previously reported [40]) bound to a potent tacrine-methylanacardate hybrid inhibitor (**TKN**, [39]).

Of particular note is the significant role played by the diphenyl moiety, which primarily facilitate binding through extensive π–π contacts with Trp82, Phe329 and Tyr332 identifying the CAS anchoring

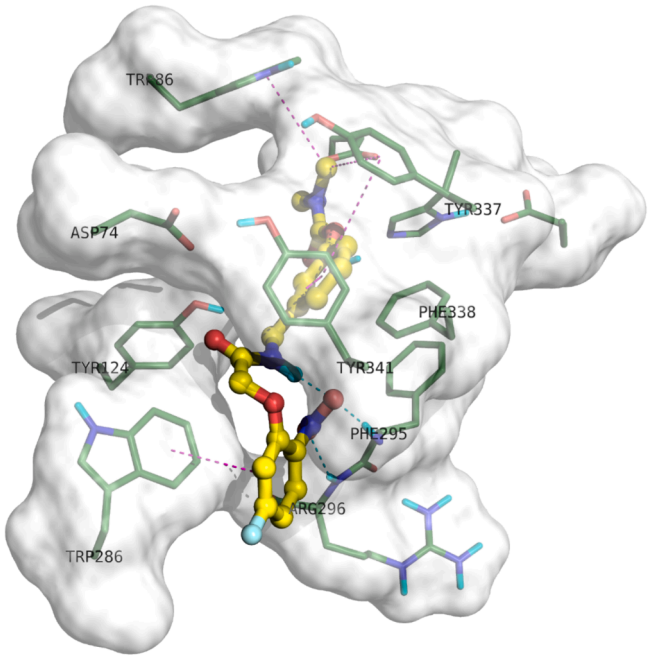

Fig. 4. Binding mode for ROS 151 to the hAChE active site. In the interaction pattern scheme hydrogen bonds and π–π stackings are depicted in cyan and magenta respectively. (For interpretation of the references to colour in this figure legend, the reader is referred to the web version of this article.)

point for BChE. Additionally, the amide group recruits a hydrogen bond pointing the NH to the CO of Pro285, while the disubstituted ring produces aromatic interactions, namely *edge-to-face* π–π stacking, involving Trp231 and the aforementioned Phe329 (Fig. 5).

Regarding the carbamate terminal fragment, both ethyl and methyl substituents are well accommodated, likely due to their accessibility at the rim of the CAS. More importantly, the interaction with the target

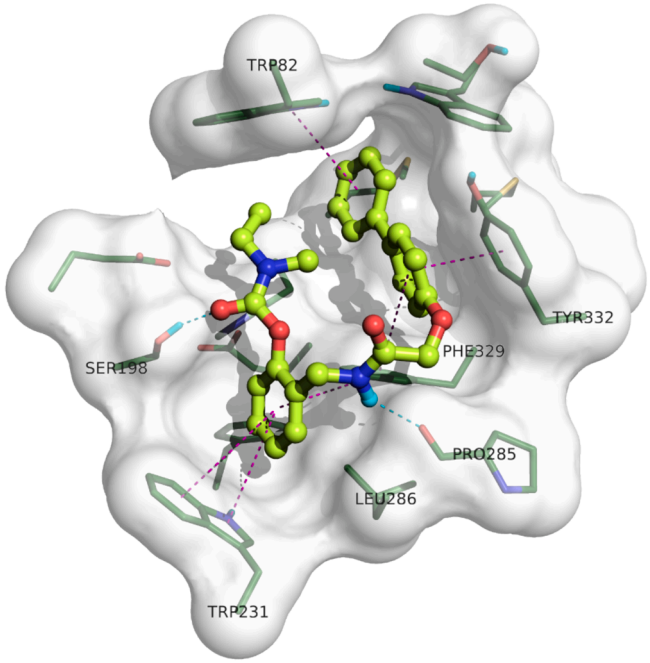

Fig. 5. Binding mode for 8 to the BChE active site. In the interaction pattern scheme hydrogen bonds and π–π stackings are depicted in cyan and magenta, respectively. (For interpretation of the references to colour in this figure legend, the reader is referred to the web version of this article.)

enzyme engaging the catalytic residue Ser198 is easier to achieve. This intriguing feature is most likely also due to a highly curved and bent ligand disposition, making possible for this inhibitor to adopt a conformation closely resembling the active one observed in the X-ray **TKN** binding mode [39].

The third docking study focused once again on compound **8**, emerging as the most potent inhibitor of hFAAH in the series. The remarkable structural feature of hFAAH is the presence of a phenylalanine and a tryptophan membrane-accessing tunnel, elongating up to an unusual (two serine residues and one lysine) catalytic triad responsible for its activity, as revealed by crystallographic data [41].

Considering this observation, compound **8** extends fully along the active site cavity. Consequently, the carbonyl oxygen of the compound comes into close and polar contact with the backbone of Phe194. Furthermore, the diphenyl aromatic terminal of the compound effectively blocks the entry channel of the amidase. This interaction involves multiple hydrophobic and aromatic contacts with Leu429, Leu433, Phe432, and Trp531 (Fig. 6).

Compound **8** was also studied for the final target investigated monoamine oxidase B (hMAO-B, [42]). Despite the inherent differences between hFAAH and hMAO-B in terms of physiological roles, folding and shape, a somewhat similar bioactive conformation was observed. As shown in Fig. 7, in hMAO-B, the ligand binds in a predominantly extended molecular arrangement. This positions the *ortho*-substituted phenyl ring in an aromatic and rectangular region just below the prosthetic FAD moiety, while the diphenyl fragment points towards the entry cavity of the enzyme.

Numerous π–π stackings and van der Waals contacts are formed, primarily involving Tyr398, Tyr435, Tyr60, and Phe343 near FAD, or

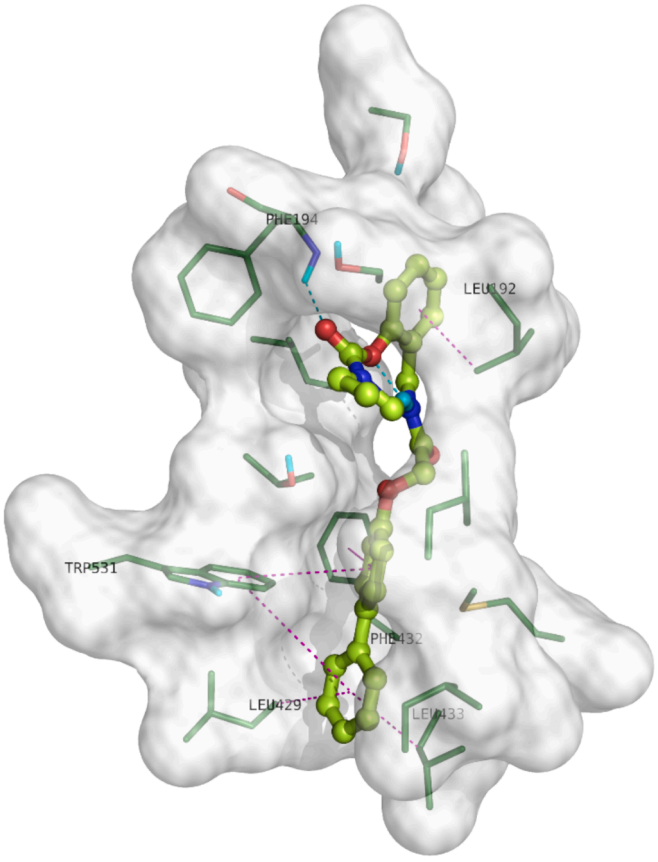

Fig. 6. Binding mode for 8 to the hFAAH active site. In the interaction pattern scheme hydrogen bonds and π-–π stackings are depicted in cyan and magenta respectively. (For interpretation of the references to colour in this figure legend, the reader is referred to the web version of this article.)

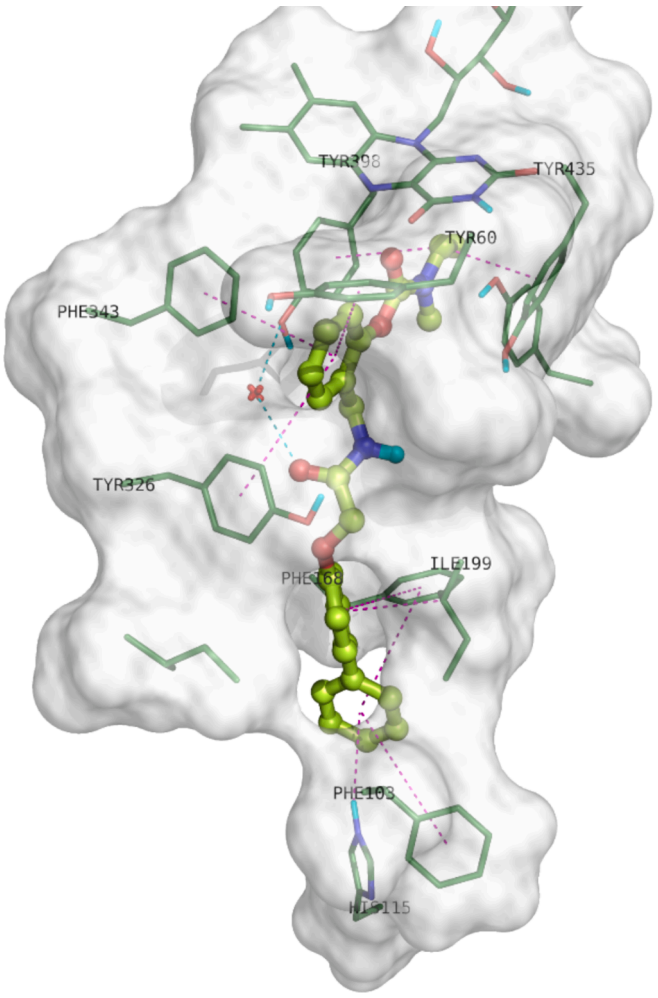

Fig. 7. Binding mode for 8 to the hMAO-B active site. In the interaction pattern scheme hydrogen bonds and π–π stackings are depicted in cyan and magenta respectively. Essential water molecules contributing to the binding are reported as red cross. (For interpretation of the references to colour in this figure legend, the reader is referred to the web version of this article.)

Phe103, His115, Phe168, Leu199, and Tyr326 close to the accessible *N*-terminal domain. Notably a water molecule bridging Tyr398 is present, enhancing the efficacy of compound **8**.

Table 4
AChE, BChE, FAAH and MAO-B ligands docking scores.

Target	Ligand	FEB[a]	ΔE[b]	EFF[c]	TAN[d]	POP[e]
AChE[f]	**5**	–11.33	0.00	–0.405	0.673	96/1000
	Donepezil	–10.83	0.05	–0.387	1.279	470/100
BChE[g]	**8**	–9.34	0.00	–0.301	0.390	339/1000
	TKN	–8.65	0.25	–0.247	1.174	21/100
FAAH[h]	**8**	–10.50	0.00	–0.339	0.354	87/1000
	JZL195	–10.22	1.02	–0.319	n.d.	20/100
MAO-B[i]	**8**	–10.86	1.27	–0.350	0.712	18/1000
	5IK	–11.92	0.60	–0.385	0.956	58/1000

[a]**FEB** Free Energy of Binding; [b]**ΔE** Energy difference between the selected pose and the relative global minimum; [c]**EFF** Ligand efficacy; [d]**TAN** Tanimoto Combo similarity coefficient with X-ray poses; [e]**POP** Cluster members population; pdb entry: 6O4W[f], 7BGC[g], 4DO3[h], 7P4F[i]. [j] for molecular structures see Figure S2; n.d. = not determined.

Overall, the docking scores reported in Table 4, validated through the ESP method (see methods), provide merit in the ranking and support the insights into experimentally determined inhibition data. Indeed, four out of five rule figures filtering the docking poses resulted below the acceptable threshold. As additional scores, in three X-ray complexes where a crystallized ligand is present (AChE, BChE, and MAO-B), a significant molecular similarity was achieved, as evidenced by the high value of the Tanimoto coefficient.

2.6. Metal chelation studies of ROS151 and Aβ aggregation inhibition activity

Considering the similarity with the already assayed copper chelator SON38 [27] and the docking calculations, the most promising compound **ROS151** was selected to be assayed in terms of biometal (Fe^{3+}, Cu^{2+}) chelating capacity, in order to evaluate its potential as metal modulator. In fact, metal chelation can be seen as a promising strategy in AD therapy, namely by promoting an improvement of metal homeostasis, inhibiting the formation of Aβ aggregates and *tau* hyperphosphorylation, as well as neuroinflammation decrease [16,17,29,43,44].

Since **ROS151** has no labile protons, the use of spectrophotometric titration technique based on pH change is not an adequate method and so the Job Plot method [45] was applied. Both Fe^{3+}/**ROS151** (pH ca 4) and Cu^{2+}/**ROS151** (pH ca 6) systems were studied by measuring the absorbance in solutions with varying metal to ligand (**ROS151**) concentration (C_M/C_L) ratio, in order to determine if metal chelation occurs and evaluate the possible stoichiometry of the respective metal complexes. Fig. 8 shows the change in absorbance values of the solution with an increase in C_M/C_L ratio, which means that **ROS151** can chelate iron and copper.

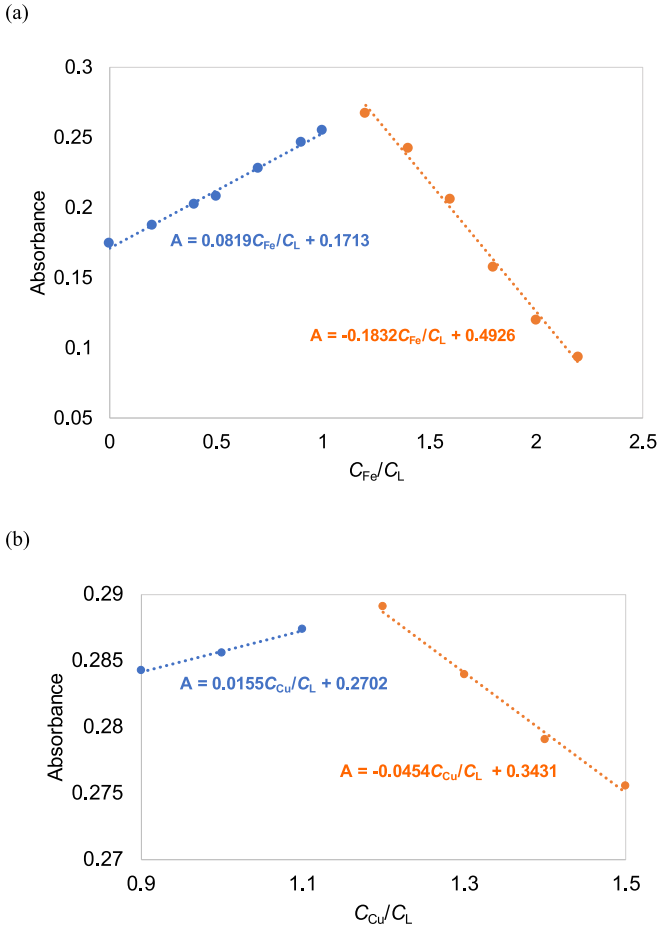

Fig. 8. Job Plot graphs showing the change in absorbance values with the metal to ligand concentration (C_M/C_L) ratio for the a) Fe^{3+}/ROS151 (pH ca 4) and b) Cu^{2+}/ROS151 (pH ca 6) systems ($C_L = 8 \times 10^{-5}$ M).

The intersection of the two straight lines shown in Fig. 8 for both M/L systems indicates a change in the linear trend at a mole fraction of 1.2, thus suggesting an approximate stoichiometry of 1:1 for the Fe^{3+}-**ROS151** and Cu^{2+}-**ROS151** complexes. Based on these experiments, it is quite likely that the intra-molecular resulting chelating core includes the NO_2 group, giving us further information about the conformation suggested by molecular docking.

Considering the promising results, the majority of the series was tested for the ability to inhibit the aggregation of $A\beta_{42}$ self-aggregation. The assays were carried out at a fixed concentration of 40 μM, but only slight effects were observed (inhibition percentages were between 9 % and 42 %, with no significant changes in the case of addition of copper to the tested solution for selected nitro-substituted compounds). These results confirm that the presence of condensed and planar heterocycles may be fundamental to confer this additional biological activity to multi-target hybrids [27,46,47]. Furthermore, the lack of labile protons in the structures, in addition to being fundamental for the quantitative determination of the chelating activity, could decrease these specific biological interactions.

However, the possible positive effect of **ROS151** (and other *ortho*-nitro substituted analogues) in the control of copper and iron dyshomeostasis to combat this particular characteristic of Alzheimer's disease remains relevant, as already assumed in the past for other multi-target hybrids such as SON38 [27].

3. Conclusions

In this study, a series of rivastigmine-like hybrids were designed, synthesized and assayed *in vitro* as inhibitors of five different enzymes, namely AChE, BChE, FAAH, MAO-A and MAO-B. To rationalize experimental results, *in silico* studies were also performed.

In general, the presence of a nitro group in *ortho* position of aryloxy ring led to an excellent inhibitory activity on AChE. In particular, hybrids **5** (**ROS151**) and **23**, sharing many structural features, had a comparable activity with donepezil and are ca. two hundred twenty-three and eighty-seven times more active than rivastigmine on AChE, with interesting inhibition kinetics, probably similar to rivastigmine. Instead, potencies on BChE were mainly in the micromolar range, without relevant spikes. Several compounds, in particular **8**, showed a good activity on FAAH. Several compounds were also inhibitors of MAO-B, with a good selectivity towards this isoform compared to MAO-A.

Regarding multi-target activity, a significative number of hybrids inhibited at least three of the tested enzymes, with **6** and **8** showing the best multi-target profiles.

Although, as expected, the ability to inhibit the aggregation of $A\beta_{42}$ was poor, **ROS151** and probably its *ortho*-nitro-substituted congeners could prove to be promising lead compounds for the search for new derivatives with these additional characteristics, given their potential as metal chelators. A specific SAR is suggested in order to include labile protons in the structure of the compounds.

The four most promising compounds (**ROS151**, **6**, **8**, **23**) exhibit pharmacokinetic properties similar to rivastigmine and donepezil. The high stability (87.7 to 92.7 % after 24 h incubation) in human plasma attributes to the properties of high half-life. PPB (79.9 to 89.3 %) is more similar to the high plasma protein binding of donepezil (96 %) than that of rivastigmine (40 %). The most important characteristic, namely the blood–brain barrier crossing ability, was confirmed by screening with the IAM chromatography showing *Pm* values greater than 1.88 (between 2.8 and 7.7) indicating CNS^+ properties. Experimental Log*P* values are between 1.9 and 3.8 supporting the assumption of BBB penetration. Cytotoxicity assays performed on the same four compounds displayed a safety profile on three different cell lines.

In conclusion, compounds **5** (**ROS151**) and **23**, despite being

derivatives of rivastigmine, present a similar inhibitory profile compared to donepezil on ChEs. On the other hand, compounds **6** and **8** are very interesting and original multi-functional promising hybrids, with comparable potency on different enzymes and good selectivity (in this case MAO-B against MAO-A is an important achievement). These new entities may represent new tools and/or lead compounds for the development of new drugs with additional targets for the treatment of Alzheimer's disease, warranting further investigation and optimization for clinical applications.

4. Experimental section

4.1. Chemistry

Chemicals were purchased from different suppliers and used without any additional purification. Percolative chromatography was conducted using as a stationary phase Geduran silica gel 60 (63–200 μm). Mass spectrometry analyses were performed by using a HP MS 6890–5973 MSD system, electron impact 70 eV, equipped with a HP ChemStation or with an Agilent LC–MS 1100 Series LC–ESI-MSD Trap System VL spectrometer. ^{1}H NMR and ^{13}C NMR spectra were recorded in the indicated deuterated solvent on Agilent VNMRS500 or Varian Mercury 300 NMR spectrometers. Chemical shifts (δ) are indicated as parts per million (ppm) and the coupling constants (J) in Hertz (Hz). NMR spectra are included in the supplementary material file (Fig. S3). Purity of all final compounds (**1**–**24**) was found to be ≥ 95 % by RP-HPLC gradient method (5–95 % ACN, acidified). Measurements were performed on a Shimadzu Prominence LC-20AD XR liquid chromatograph device (Shimadzu Corporation, Tokyo, Japan) with Acclaim™ 120 C18 column (5 μm, 4.6 × 150 mm, Thermofischer, Dreieich, Germany). The gradient (0–7 min 5–95 % B; 7–11 min 95 % B) solvent B was acetonitrile (0.1 % formic acid) and solvent A water (0.1 % formic acid). Flow rate was set at 1.0 mL/min and the column oven was maintained at 25° C. The samples were prepared by diluting the stock solutions with water (1:1 *v/v*). Injection volume was 5 μL. Sample traces with indication of purities are included in the supplementary material file (Fig. S4). Exact mass analyses of final compounds were within the accepted values compared to the theoretical values. Melting points are uncorrected and were measured on a Gallenkamp electrothermal apparatus (Fisons Erba Science Ltd., Guildford, UK) in open capillaries.

4.2. Preparation of cyanophenyl dialkylcarbamates 25a-32a. General procedure

The appropriate cyanophenol (3.63 mmol, 1 eq) and the suitable carbamoyl chloride (3.7 mmol, 1.02 eq) were added to triethylamine (2 mL). The reaction mixture was refluxed for 5 h and then stirred at room temperature overnight. The mixture was diluted with CH_2Cl_2 and the organic portion was washed with 1 N NaOH (three times), dried over anhydrous Na_2SO_4, filtered and concentrated to dryness, obtaining a crude, that was purified by chromatography column (eluent 100 % CH_2Cl_2), to give the title compounds.

4.2.1. 2-Cyanophenyl diethylcarbamate (**25a**)

Yellow oil, yield 61 %. Starting from diethylcarbamoyl chloride and 2-cyanophenol. ^{1}H NMR (300 MHz, $CDCl_3$) δ: 1.13–1.47 (m, 6H, $CH_2\underline{CH_3}$), 3.29–3.57 (m, 4H, $\underline{CH_2}CH_3$), 7.19–7.45 (m, 2H aromatics), 7.53–7.76 (m, 2H aromatics). GC–MS *m/z* (%): 218 (4) $[M]^+$, 100 (100), 72 (53).

4.2.2. 2-Cyanophenyl ethyl(methyl)carbamate (**26a**)

Yellow oil, yield 54 %. Starting from *N*-ethyl-*N*-methyl carbamoyl chloride and 2-cyanophenol. ^{1}H NMR (300 MHz, $CDCl_3$) δ: 1.15–1.37 (m, 3H, $CH_2\underline{CH_3}$), 2.91–3.23 (m, 3H, $\underline{CH_3}$), 3.35–3.60 (m, 2H, $\underline{CH_2}CH_3$), 7.23–7.30 (m, 1H aromatic), 7.36–7.45 (m, 1H aromatic) and 7.54–7.68 (m, 2H aromatics). GC–MS *m/z* (%): 204 (6) $[M]^+$, 86 (100), 58 (65).

4.2.3. 4-Cyanophenyl diethylcarbamate (**27a**)

Yellow oil, yield 58 %. Starting from diethylcarbamoyl chloride and 4-cyanophenol. ^{1}H NMR (300 MHz, $CDCl_3$) δ: 1.16–1.34 (m, 6H, $CH_2\underline{CH_3}$), 3.31–3.51 (m, 4H, $\underline{CH_2}CH_3$), 7.21–7.34 (m, 2H aromatics), 7.61–7.73 (m, 2H aromatics). GC–MS *m/z* (%): 218 (0,07) $[M]^+$, 100 (100), 72 (56).

4.2.4. 4-Cyanophenyl dimethylcarbamate (**28a**)

Yellow solid, yield 42 %. Starting from dimethyl carbamoyl chloride and 4-cyanophenol. ^{1}H NMR (300 MHz, $CDCl_3$) δ: 3.02 (s, 3H, $\underline{CH_3}$), 3.11 (s, 3H, $\underline{CH_3}$), 7.21–7.31 (m, 2H aromatics), 7.62–7.70 (m, 2H aromatics). GC–MS *m/z* (%): 190 (4) $[M]^+$, 72 (100).

4.2.5. 4-Cyanophenyl ethyl(methyl)carbamate (**29a**)

Yellow oil, yield 55 %. Starting from *N*-ethyl-*N*-methyl carbamoyl chloride and 4-cyanophenol. ^{1}H NMR (300 MHz, $CDCl_3$) δ: 1.16–1.30 (m, 3H, $CH_2\underline{CH_3}$), 2.95–3.13 (m, 3H, $\underline{CH_3}$), 3.35–3.53 (m, 2H, $\underline{CH_2}CH_3$), 7.21–7.30 (m, 2H aromatics), 7.62–7.71 (m, 2H aromatics). GC–MS *m/z* (%): 204 (3) $[M]^+$, 86 (100), 58 (66).

4.2.6. 3-Cyanophenyl diethylcarbamate (**30a**)

Yellow oil, yield 43 %. Starting from diethylcarbamoyl chloride and 3-cyanophenol. ^{1}H NMR (300 MHz, $CDCl_3$) δ: 1.15–1.39 (m, 6H, $CH_2\underline{CH_3}$), 3.32–3.50 (m, 4H, $\underline{CH_2}CH_3$), 7.35–7.53 (m, 4H aromatics). GC–MS *m/z* (%): 218 (1) $[M]^+$, 100 (100), 72 (57).

4.2.7. 3-Cyanophenyl dimethylcarbamate (**31a**)

Yellow solid, yield 65 %. Starting from dimethyl carbamoyl chloride and 3-cyanophenol. ^{1}H NMR (300 MHz, $CDCl_3$) δ: 3.02 (s, 3H, $\underline{CH_3}$), 3.08 (s, 3H, $\underline{CH_3}$), 7.35–7.52 (m, 4H aromatics). GC–MS *m/z* (%): 190 (4) $[M]^+$, 90 (3), 72 (100).

4.2.8. 3-Cyanophenyl ethyl(methyl)carbamate (**32a**)

Yellow oil, yield 31 %. Starting from *N*-ethyl-*N*-methyl carbamoyl chloride and 3-cyanophenol. ^{1}H NMR (300 MHz, $CDCl_3$) δ: 0.94–1.45 (m, 3H, $CH_2\underline{CH_3}$), 2.92–3.12 (m, 3H, $\underline{CH_3}$), 3.29–3.56 (m, 2H, $\underline{CH_2}CH_3$), 7.30–7.59 (m, 4H aromatics). GC–MS *m/z* (%): 204 (2) $[M]^+$, 86 (100), 58 (73).

4.3. Preparation of free amines **25**–**26**

The suitable *ortho*-carbamate cyano-derivate **25a–26a** (3.89 mmol, 1 eq), previously dissolved in absolute EtOH (24 mL), was hydrogenated at a pressure of 2 atm in the presence of 10 % Pd/C (1.39 mmol, 0.45 eq) overnight. The catalyst was filtered off, the solvent was removed *in vacuo* and the resulting oil was purified by a first column chromatography (eluent EtOAc/MeOH 95:5) and a second one (eluent CH_2Cl_2/MeOH 95:5) to obtain the title compounds.

4.3.1. 2-(Aminomethyl)phenyl diethylcarbamate (**25**)

Yellow oil, yield 23 %. Starting from 2-cyanophenyl diethylcarbamate (**25a**). ^{1}H NMR (300 MHz, $CDCl_3$) δ: 1.18–1.31 (m, 6H, $CH_2\underline{CH_3}$), 3.35–3.50 (m, 4H, $\underline{CH_2}CH_3$), 3.78 (s, 2H, $\underline{CH_2}NH_2$), 7.05–7.10 (m, 1H aromatic), 7.17–7.28 (m, 2H aromatics), 7.34–7.38 (m, 1H aromatic), GC–MS *m/z* (%): 222 (1) $[M]^+$; 122 (19); 106 (43); 100 (85); 72 (100).

4.3.2. 2-(Aminomethyl)phenyl ethyl(methyl)carbamate (**26**)

Yellow oil, yield 26 %. Starting from 2-cyanophenyl ethyl(methyl) carbamate (**26a**). ^{1}H NMR (300 MHz, $CDCl_3$) δ: 1.16–1.29 (m, 3H, $CH_2\underline{CH_3}$), 2.98 and 3.10 (s, 3H, $\underline{CH_3}$), 3.34–3.57 (m, 2H, $\underline{CH_2}CH_3$), 6.94–7.15 (m, 2H aromatic) and 7.22–7.38 (m, 2H aromatics), GC–MS *m/z* (%): 208 (65) $[M]^+$; 122 (42); 86 (79); 58 (100); 44 (69).

4.4. Preparation of free amines 27–32

The suitable *meta*- or *para*-carbamate cyano-derivate **27a–32a** (2.89 mmol, 1 eq), previously dissolved in MeOH (28 mL), was hydrogenated at a pressure of 4 atm in the presence of 10 % Pd/C (4.16 mmol, 1.46 eq) for 4 h. The catalyst was filtered off, the solvent was removed *in vacuo* and the resulting oil was purified with a first column chromatography (eluent CH_2Cl_2/MeOH 95:5) and a second one (eluent EtOAc/MeOH, 95:5) to obtain the title compounds.

4.4.1. 4-(Aminomethyl)phenyl diethylcarbamate (27)

Yellow oil, yield 47 %. Starting from 4-cyanophenyl diethylcarbamate (**27a**). ^{1}H NMR (300 MHz, $CDCl_3$) δ: 1.13–1.31 (m, 6H, $CH_2\underline{CH_3}$), 3.41 (m, 4H, $\underline{CH_2}CH_3$), 3.85 (s, 2H, $\underline{CH_2}NH_2$), 7.04–7.11 (m, 2H aromatics), 7.26–7.33 (m, 2H aromatics). GC–MS *m/z* (%): 222 (5) $[M]^+$; 100 (100); 72 (56).

4.4.2. 4-(Aminomethyl)phenyl dimethylcarbamate (28)

Yellow oil, yield 45 %. Starting from 4-cyanophenyl dimethylcarbamate (**28a**). ^{1}H NMR (300 MHz, $CDCl_3$) δ: 2.98 (s, 3H, $\underline{CH_3}$), 3.11 (s, 3H, $\underline{CH_3}$), 3.89 (s, 2H, $\underline{CH_2}NH_2$), 7.01–7.17 (m, 2H aromatics), 7.32–7.47 (m, 2H aromatics). GC–MS *m/z* (%): 194 (4) $[M]^+$; 106 (26); 72 (100).

4.4.3. 4-(Aminomethyl)phenyl ethyl(methyl)carbamate (29)

Yellow oil, yield 43 %. Starting from 4-cyanophenyl ethyl(methyl) carbamate (**29a**). ^{1}H NMR (300 MHz, $CDCl_3$) δ: 1.13–1.33 (m, 3H, $CH_2\underline{CH_3}$), 3.02 (s, 3H, $\underline{CH_3}$), 3.34–3.55 (m, 2H, $\underline{CH_2}CH_3$), 3.83 (d, J = 15.1 Hz, 2H, $\underline{CH_2}NH_2$), 7.00–7.15 (m, 2H aromatics), 7.28–7.38 (m, 2H aromatics). GC–MS *m/z* (%): 208 (4) $[M]^+$; 106 (22); 86 (100); 58 (67).

4.4.4. 3-(Aminomethyl)phenyl diethylcarbamate (30)

Yellow oil, yield 51 %. Starting from 3-cyanophenyl diethylcarbamate (**30a**). ^{1}H NMR (300 MHz, $CDCl_3$) δ: 0.99–1.44 (m, 6H, $CH_2\underline{CH_3}$), 3.24–3.57 (m, 4H, $\underline{CH_2}CH_3$), 3.87 (s, 2H, $\underline{CH_2}NH_2$), 6.93–7.18 (m, 2H aromatics), 7.29–7.52 (m, 2H aromatics). GC–MS *m/z* (%): 222 (5) $[M]^+$; 100 (100); 72 (56).

4.4.5. 3-(Aminomethyl)phenyl dimethyl carbamate (31)

Yellow oil, yield 49 %. Starting from 3-cyanophenyl dimethylcarbamate (**31a**). ^{1}H NMR (300 MHz, $CDCl_3$) δ: 3.01 (s, 3H, $\underline{CH_3}$), 3.09 (s, 3H, $\underline{CH_3}$), 3.85 (s, 2H, $\underline{CH_2}NH_2$), 6.91–7.03 (m, 1H aromatic), 7.08–7.16 (m, 2H aromatics), 7.25–7.34 (m, 1H aromatic). GC–MS *m/z* (%): 194 (4) $[M]^+$; 106 (26); 72 (100).

4.4.6. 3-(Aminomethyl)phenyl ethyl(methyl)carbamate (32)

Yellow oil, yield 71 %. Starting from 3-cyanophenyl ethyl(methyl) carbamate (**32a**). ^{1}H NMR (300 MHz, $CDCl_3$) δ: 1.13–1.28 (m, 3H, $CH_2\underline{CH_3}$), 2.95–3.09 (m, 3H, $\underline{CH_3}$), 3.28–3.54 (m, 2H, $\underline{CH_2}CH_3$), 6.92–7.04 (m, 1H aromatic), 7.07–7.19 (m, 2H aromatics), 7.27–7.35 (m, 1H aromatic). GC–MS *m/z* (%): 208 (6) $[M]^+$; 106 (23); 86 (100); 58 (82).

4.5. Preparation of ethyl phenoxy acetate derivatives 33a–35a. General procedure

The appropriate commercial phenol (11.52 mmol, 1 eq) was added to a solution of sodium ethoxide, prepared dissolving Na (11.52 mmol, 1 eq) in absolute ethanol (55 mL), and the mixture was stirred for 30 min. Subsequently, a solution of ethyl bromoacetate (11.52 mmol, 1 eq) in absolute ethanol (40 mL) was added dropwise and the reaction mixture was refluxed for 24 h. The solvent was removed under reduced pressure, and the crude was treated with diethyl ether and washed with 0.5 N NaOH and brine, dried over anhydrous Na_2SO_4, filtered and concentrated to dryness, obtaining the title compounds **33a–35a**. Chemical characterization is reported in a previous work of the same group [27].

4.6. Preparation of phenoxy acetic acid derivatives 33–35. General procedure

1 N NaOH (67.6 mmol, 10 eq) was added to a solution of the suitable ethyl phenoxy acetate derivatives (**33a–35a**) (6.76 mmol, 1 eq) dissolved in THF (45 mL). The reaction mixture was stirred for 5 h at room temperature. Then, the organic solvent was removed *in vacuo*, the aqueous residue was acidified with 6 n HCl and extracted with diethyl ether (three times). The organic portions were collected and washed with brine, dried over anhydrous Na_2SO_4, filtered and concentrated to dryness, affording compounds 33–35. Chemical characterization is reported in a previous work of the same group [27]

4.7. Preparation of the final compounds 1–24. General procedure

The suitable free amine **25–32** (0.45, 2 eq) was dissolved in CH_2Cl_2 (5 mL), then the appropriate phenoxy acetic acid derivatives **33–36** (0.675 mmol, 3 eq), 1-hydroxybenzotriazole hydrate (HOBt, 0.23 mmol, 1 eq) and *N,N′*-diisopropylcarbodiimide (DIC, 0.9 mmol, 4 eq), were added in that order. The reaction mixture was stirred for 16 h at room temperature, then it was filtered through a Büchner funnel, the solvent was removed *in vacuo*. The resulting crude was purified through column chromatography.

4.7.1. 2-((2-(5-Fluoro-2-nitrophenoxy)acetamido)methyl)phenyl diethylcarbamate (1)

White solid, yield 23 %; m.p. = 119–120 °C. Starting from 2-(5-Fluoro-2-nitrophenoxy)acetic acid (**33**) and 2-(aminomethyl)phenyl diethylcarbamate (**25**), eluent: CH_2Cl_2/MeOH 95:5. ^{1}H NMR (500 MHz, $CDCl_3$) δ: 1.15–1.31 (m, 6H, $CH_2\underline{CH_3}$), 3.35–3.43 (m, 4H, $\underline{CH_2}CH_3$), 4.54 (d, J = 5.9 Hz, 2H, $NH\underline{CH_2}CH$), 4.60 (s, 2H, $O\underline{CH_2}CO$), 6.70–6.84 (m, 2H aromatics), 7.08–7.12 (m, 1H aromatic), 7.17–7.23 (m, 1H aromatic), 7.27–7.33 (m, NH), 7.40–7.50 (m, 2H aromatics), 8.04–8.10 (m, 1H aromatic). ^{13}C NMR (126 MHz, $CDCl_3$) δ: 13.35, 14.29, 38.12, 42.05, 42.32, 68.16, 102.68 (d, $J_{2,C\text{-}F}$ = 25.2 Hz), 108.91 (d, $J_{2,C\text{-}F}$ = 21.4 Hz), 122.63, 125.85, 128.89, 129.70, 129.91, 149.67, 165.79. HRMS ($C_{20}H_{22}FN_3O_6$ + Na^+): calculated 442.1385 found 442.1391.

4.7.2. 2-((2-(5-Fluoro-2-nitrophenoxy)acetamido)methyl)phenyl ethyl (methyl)carbamate (2)

White solid, yield 18 %; m.p. = 109–111 °C. Starting from 2-(5-Fluoro-2-nitrophenoxy)acetic acid (**33**) and 2-(aminomethyl)phenyl ethyl(methyl)carbamate (**26**), eluent:: *n*-hexane/AcOEt 7:3, then CH_2Cl_2/MeOH 99:1. ^{1}H NMR (300 MHz, $CDCl_3$) δ: 1.16–1.32 (m, 3H, $CH_2\underline{CH_3}$), 2.87–3.18 (m, 3H, CH_3), 3.33–3.60 (m, 2H, $\underline{CH_2}CH_3$), 4.48–4.68 (m, 4H, 2H $NH\underline{CH_2}CH$ + 2H $O\underline{CH_2}CO$), 6.68–6.87 (m, 2H aromatics), 7.04–7.34 (m, 3H aromatics), 7.38–7.54 (m, 2H, 1H aromatic + 1H NH). 8.00–8.17 (m, 1H aromatic). ^{13}C NMR (126 MHz, $CDCl_3$) δ: 12.45, 13.27, 33.87, 34.31, 38.19, 44.22, 68.11, 102.67 (d, $J_{2,C\text{-}F}$ = 27 Hz), 108.87 (d, $J_{2,C\text{-}F}$ = 23.3 Hz), 122.69 (d, $J_{3,C\text{-}F}$ = 9.9 Hz), 125.90, 128.97, 129.78, 153.01, 154.25 (d, $J_{3,C\text{-}F}$ = 11.1 Hz), 165.89 165.93 (d, $J_{1,C\text{-}F}$ = 127 Hz). HRMS ($C_{19}H_{20}FN_3O_6$ + Na^+): calculated 428.1234 found 428.1229.

4.7.3. 4-((2-(5-Fluoro-2-nitrophenoxy)acetamido)methyl)phenyl diethylcarbamate (3)

White solid, yield 52 %; m.p. = 162–164 °C. Starting from 2-(5-Fluoro-2-nitrophenoxy)acetic acid (**33**) and 4-(aminomethyl)phenyl diethylcarbamate (**27**), eluent: CH_2Cl_2/MeOH 95:5. ^{1}H NMR (300 MHz, $CDCl_3$) δ: 1.16–1.30 (m, 6H, $CH_2\underline{CH_3}$), 3.31–3.49 (m, 4H, $\underline{CH_2}CH_3$), 4.55 (d, J = 6.0 Hz, 2H, $NH\underline{CH_2}CH$), 4.62 (s, 2H, $O\underline{CH_2}CO$), 6.71–6.89 (m, 2H aromatics), 7.05–7.14 (m, 2H aromatics), 7,29—7.39 (m, 2H aromatics), 7.49–7.59 (bs, NH), 8.07–8.15 (m, 1H aromatic). ^{13}C NMR (126 MHz, $CDCl_3$) δ: 14.21, 13.35, 41.86, 42.22, 42.64, 68.03, 102.63 (d, $J_{2,C\text{-}F}$ = 27 Hz), 108.99 (d, $J_{2,C\text{-}F}$ = 23.2 Hz), 122.08, 128.74, 129.13 (d, $J_{3,C\text{-}F}$ = 11.4 Hz), 134.24, 151.00, 152.96 (d, $J_{3,C\text{-}F}$ = 11.2 Hz), 154.08, 165.81,

166.14 (d, $J_{1,C\text{-}F}$ = 259.1 Hz). HRMS ($C_{20}H_{22}FN_3O_6$ + Na^+): calculated 442.1385 found 442.1397.

4.7.4. 3-((2-(5-Fluoro-2-nitrophenoxy)acetamido)methyl)phenyl diethylcarbamate (4)

White solid, yield 43 %; m.p. = 110–112 °C. Starting from 2-(5-Fluoro-2-nitrophenoxy)acetic acid (**33**) and 3-(aminomethyl)phenyl diethylcarbamate (**30**), eluent: 100 % CH_2Cl_2, then 100 % AcOEt. ^{1}H NMR (300 MHz, $CDCl_3$) δ: 1.17–1.28 (m, 6H, $CH_2\underline{CH_3}$), 3.32–3.49 (m, 4H, $\underline{CH_2}CH_3$), 4.56 (d, J = 6.1 Hz, 2H, NH$\underline{CH_2}$CH), 4.63 (s, 2H, O$\underline{CH_2}$CO), 6.73–6.87 (m, 2H aromatics), 7.03–7.12 (m, 2H aromatics), 7.14–7.20 (m, 1H aromatic), 7.30–7.37 (m, 1H aromatic), 7.50–7.60 (m, NH), 8.09–8.16 (m, 1H aromatic). ^{13}C NMR (126 MHz, $CDCl_3$) δ: 13.35, 14.21, 41.88, 42.22, 42.84, 68.04, 102.64 (d, $J_{2,C\text{-}F}$ = 27 Hz), 108.98 (d, $J_{2,C\text{-}F}$ = 23.3 Hz), 121.17, 124.35, 129.09 (d, $J_{3,C\text{-}F}$ = 11.3 Hz), 129.55, 138.85, 151.77, 152.95 (d, $J_{3,C\text{-}F}$ = 11.2 Hz), 154.06, 165.92, 166.12 (d, $J_{1,C\text{-}F}$ = 259.2 Hz). HRMS ($C_{20}H_{22}FN_3O_6$ + Na^+): calculated 442.1385 found 442.1400.

4.7.5. 3-((2-(5-Fluoro-2-nitrophenoxy)acetamido)methyl)phenyl dimethylcarbamate (5)

White solid, yield 40 %; m.p. = 133–135 °C. Starting from 2-(5-Fluoro-2-nitrophenoxy)acetic acid (**33**) and 3-(aminomethyl)phenyl dimethylcarbamate (**31**), eluent: *n*-hexane/AcOEt, 7:3, then 100 % CH_2Cl_2. ^{1}H NMR (300 MHz, $CDCl_3$) δ: 3.00 (s, 3H, CH_3), 3.09 (s, 3H, CH_3), 4.56 (d, J = 6.1 Hz, 2H, NH$\underline{CH_2}$CH), 4.63 (s, 2H, O$\underline{CH_2}$CO), 6.73–6.88 (m, 2H aromatics), 7.01–7.21 (m, 3H aromatics), 7.29–7.39 (m, 1H aromatic), 7.49–7.63 (m, NH), 8.06–8.17 (m, 1H aromatic). ^{13}C NMR (126 MHz, $CDCl_3$) δ: 36.44, 36.67, 42.81, 67.96, 102.64 (d, $J_{2,C\text{-}F}$ = 27 Hz), 108.99 (d, $J_{2,C\text{-}F}$ = 23.3 Hz), 121.12, 124.44, 129.10 (d, $J_{3,C\text{-}F}$ = 11.4 Hz), 129.57, 138.92, 151.77, 152.95 (d, $J_{3,C\text{-}F}$ = 11.2 Hz), 154.74, 165.95, 166.12 (d, $J_{1,C\text{-}F}$ = 259.2 Hz). HRMS ($C_{20}H_{22}FN_3O_6$ + Na^+): calculated 414.1077 found 414.1110.

4.7.6. 3-((2-(5-Fluoro-2-nitrophenoxy)acetamido)methyl)phenyl ethyl (methyl)carbamate (6)

White solid, yield 20 %; m.p. = 105–107 °C. Starting from 2-(5-Fluoro-2-nitrophenoxy)acetic acid (**33**) and 3-(aminomethyl)phenyl ethyl(methyl)carbamate (**32**), eluent: *n*-hexane/AcOEt 9:1, then 100 % CH_2Cl_2. ^{1}H NMR (300 MHz, $CDCl_3$) δ: 1.14–1.30 (m, 3H, $CH_2\underline{CH_3}$), 2.92–3.10 (s, 3H, CH_3), 3.34–3.52 (m, 4H, $\underline{CH_2}CH_3$), 4.56 (d, J = 6.1 Hz, 2H, NH$\underline{CH_2}$CH), 4.64 (s, 2H, O$\underline{CH_2}$CO), 6.72–6.88 (m, 2H aromatics), 6.98–7.22 (m, 3H aromatics), 7.30–7.37 (m, 1H aromatic), 7.49–7.63 (m, NH), 8.04–8.18 (m, 1H aromatic). ^{13}C NMR (126 MHz, $CDCl_3$) δ: 12.42, 13.19, 33.79, 34.21, 42.83, 44.13. 68.04, 102.64 (d, $J_{2,C\text{-}F}$ = 27 Hz), 108.98 (d, $J_{2,C\text{-}F}$ = 23.3 Hz), 121.14, 124.40, 129.09 (d, $J_{3,C\text{-}F}$ = 11.4 Hz), 129.57, 135.23, 138.88, 151.77, 152.95 (d, $J_{3,C\text{-}F}$ = 11.3 Hz), 154.38, 165.94, 166.12 (d, $J_{1,C\text{-}F}$ = 259.2 Hz). HRMS ($C_{19}H_{20}FN_3O_6$ + Na^+): calculated 428.1234 found 428.1230.

4.7.7. 2-((2-([1,1′-Biphenyl]-4-yloxy)acetamido)methyl)phenyl diethylcarbamate (7)

White solid, yield 17 %; m.p. = 104–106 °C. Starting from 2-([1,1′-biphenyl]-4-yloxy)acetic acid (**34**) and 2-(aminomethyl)phenyl diethylcarbamate (**25**), eluent: CH_2Cl_2/MeOH 95:5. ^{1}H NMR (300 MHz, $CDCl_3$) δ: 1.10–1.36 (m, 6H, $CH_2\underline{CH_3}$), 3.30–3.51 (m, 4H, $\underline{CH_2}CH_3$), 4.50 (d, J = 5.6 Hz, 2H, NH$\underline{CH_2}$CH), 4.54 (s, 2H, O$\underline{CH_2}$CO), 6.96–7.23 (m, 4H aromatics), 7.27–7.65 (m, 10*H*, 9H aromatics + 1H NH). ^{13}C NMR (126 MHz, $CDCl_3$) δ: 13.32, 14.32, 38.36, 42.08, 42.47, 67.26, 114.99, 122.70, 126.13, 126.74, 128.28, 128.75, 129.17, 130.13, 130.34, 135.00, 140.44, 149.99, 154.51, 156.80, 167.87. HRMS ($C_{26}H_{28}N_2O_4$ + Na^+): calculated 455.1941 found 455.1952.

4.7.8. 2-((2-([1,1′-Biphenyl]-4-yloxy)acetamido)methyl)phenyl ethyl (methyl)carbamate (8)

White solid, yield 26 %; m.p. = 103–105 °C. Starting from 2-([1,1′-biphenyl]-4-yloxy)acetic acid (**34**) and 2-(aminomethyl)phenyl ethyl (methyl)carbamate (**26**), eluent: *n*-hexane/AcOEt, 7:3, then CH_2Cl_2/MeOH 97:3. ^{1}H NMR (300 MHz, $CDCl_3$) δ: 1.07–1.34 (m, 3H, $CH_2\underline{CH_3}$), 2.91–3.11 (m, 3H, CH_3), 3.30–3.54 (m, 2H, $\underline{CH_2}CH_3$), 4.46–4.56 (m, 4H, 2H NH$\underline{CH_2}$CH + 2H O$\underline{CH_2}$CO), 6.96–7.26 (m, 5H, 4H aromatics + 1H NH), 7.28–7.59 (m, 9H aromatics). ^{13}C NMR (126 MHz, $CDCl_3$) δ: 12.39, 13.27, 33.90, 34.35, 38.42, 44,17, 44.29, 67.34, 115.00, 122.73, 126.10, 126.15, 126.74, 128.30, 128.75, 129.14, 130.06, 130.26, 135.04, 140.42, 149.94, 154.68, 156.79, 167.83. HRMS ($C_{25}H_{26}N_2O_4$ + Na^+): calculated 441.1790 found 441.1802.

4.7.9. 4-((2-([1,1′-Biphenyl]-4-yloxy)acetamido)methyl)phenyl diethylcarbamate (9)

White solid, yield 45 %; m.p. = 120–122 °C. Starting from 2-([1,1′-biphenyl]-4-yloxy)acetic acid (**34**) and 4-(aminomethyl)phenyl diethylcarbamate (**27**), eluent: 100 % CH_2Cl_2. ^{1}H NMR (300 MHz, $CDCl_3$) δ: 1.16–1.29 (m, 6H, $CH_2\underline{CH_3}$), 3.33–3.50 (m, 4H, $\underline{CH_2}CH_3$), 4.54 (d, J = 5.9 Hz, 2H, NH$\underline{CH_2}$CH), 4.60 (s, 2H, O$\underline{CH_2}$CO), 6.81–6.91 (bs, 1H, NH), 6.94–7.14 (m, 4H aromatics), 7.26–7.60 (m, 9H aromatics). ^{13}C NMR (126 MHz, $CDCl_3$) δ: 13.38, 14.24, 41.88, 42.26, 42.54, 67.43, 114.99, 122.11, 126.78, 126.96, 128.42, 128.76, 128.79, 134.41, 135.24, 140.36, 151.00, 154.14, 156.63, 168.05. HRMS ($C_{26}H_{28}N_2O_4$ + Na^+): calculated 455.1941 found 455.1946.

4.7.10. 3-((2-([1,1′-Biphenyl]-4-yloxy)acetamido)methyl)phenyl diethylcarbamate (10)

White solid, yield 2 %; m.p. = 76–77 °C. Starting from 2-([1,1′-biphenyl]-4-yloxy)acetic acid (**34**) and 3-(aminomethyl)phenyl diethylcarbamate (**30**), eluent: 100 % CH_2Cl_2. ^{1}H NMR (300 MHz, $CDCl_3$) δ: 1.12–1.32 (m, 6H, $CH_2\underline{CH_3}$), 3.26–3.50 (m, 4H, $\underline{CH_2}CH_3$), 4.56 (d, J = 6 Hz, 2H, NH$\underline{CH_2}$CH), 4.59 (s, 2H, O$\underline{CH_2}$CO), 6.95–7.15 (m, 5H, 4H aromatics + 1H NH), 7.24–7.60 (m, 9H aromatics). ^{13}C NMR (126 MHz, $CDCl_3$) δ: 13.35, 14.22, 41.88, 42.26, 42.69, 67.43, 114.98, 121.23, 124.46, 126.96, 128.42, 128.75, 129.57, 135.27, 139.04, 140.36, 151.75, 154.11, 156.60, 168.13. HRMS ($C_{26}H_{28}N_2O_4$ + Na^+): calculated 455.1941 found 455.1942.

4.7.11. 3-((2-([1,1′-Biphenyl]-4-yloxy)acetamido)methyl)phenyl dimethylcarbamate (11)

White solid, yield 49 %; m.p. = 94–96 °C. Starting from 2-([1,1′-biphenyl]-4-yloxy)acetic acid (**34**) and 3-(aminomethyl)phenyl dimethylcarbamate (**32**), eluent: CH_2Cl_2/MeOH 95:5. ^{1}H NMR (300 MHz, $CDCl_3$) δ: 2.99 (s, 3H, CH_3), 3.07 (s, 3H, CH_3), 4.55 (d, J = 6.0 Hz, 2H, NH$\underline{CH_2}$CH), 4.59 (s, 2H, O$\underline{CH_2}$CO), 6.89–7.15 (m, 6H, 5H aromatics + 1H NH), 7.27–7.60 (m, 8H aromatics).

^{13}C NMR (126 MHz, $CDCl_3$) δ: 36.41, 36.68, 42.63, 67.44, 115.00, 121.14, 124.52, 126.77, 126.97, 128.41, 128.77, 129.56, 135.23, 139.18, 140.36, 151.77, 154.77, 156.63, 168.13. HRMS ($C_{24}H_{24}N_2O_4$ + Na^+): calculated 427.1628 found 427.1629.

4.7.12. 3-((2-([1,1′-Biphenyl]-4-yloxy)acetamido)methyl)phenyl ethyl (methyl)carbamate (12)

White solid, yield 53 %; m.p. = 93–95 °C. Starting from 2-([1,1′-biphenyl]-4-yloxy)acetic acid (**34**) and 3-(aminomethyl)phenyl ethyl (methyl)carbamate (**26**), eluent: CH_2Cl_2/MeOH 98:2; then *n*-hexane/AcOEt 7:3. ^{1}H NMR (300 MHz, $CDCl_3$) δ: 1.16–1.26 (m, 3H, $CH_2\underline{CH_3}$), 2.90–3.10 (m, 3H, CH_3), 3.34–3.49 (m, 2H, $\underline{CH_2}CH_3$), 4.56 (d, J = 6.0 Hz, 2H, NH$\underline{CH_2}$CH), 4.60 (s, 2H, O$\underline{CH_2}$CO), 6.90–7.16 (m, 6H, 5H aromatics + 1H NH), 7.27–7.47 (m, 4H aromatics), 7.27–7.47 (m, 4H aromatics). ^{13}C NMR (126 MHz, $CDCl_3$) δ: 13.21, 13.44, 33.78, 34.23, 42.66, 44.07, 67.43, 114.98, 121.19, 124.51, 126.77, 126.96, 128.42, 128.76, 129.58, 135.26, 139.10, 140.35, 151.76, 156.61, 168.11. HRMS ($C_{25}H_{26}N_2O_4$ + Na^+): calculated 441.1785 found 441.1798.

4.7.13. 2-((2-(4-Chlorophenoxy)acetamido)methyl)phenyl ethyl(methyl) carbamate (13)

White solid, yield 21 %; m.p. = 79–81 °C. Starting from 2-(4-chlorophenoxy)acetic acid (**36**) and 2-(aminomethyl)phenyl ethyl(methyl) carbamate (**26**), eluent: *n*-hexane/AcOEt 7:3, then CH_2Cl_2 99:1. ^{1}H NMR (300 MHz, $CDCl_3$) δ: 1.08–1.32 (m, 3H, $CH_2\underline{CH_3}$), 2.90–3.11 (m, 3H, CH_3), 3.27–3.54 (m, 2H, $\underline{CH_2}CH_3$), 4.41–4.51 (m, 4H, 2H $NH\underline{CH_2}CH$ + 2H $O\underline{CH_2}CO$), 6.91–6.89 (m, 2H aromatics),7.04–7.13 (m, 1H aromatic), 7.16–7.26 (m, 4H, 3H aromatics + 1H NH), 7.29–7.38 (m, 2H aromatics). ^{13}C NMR (126 MHz, $CDCl_3$) δ: 12.36, 13.25, 33.91, 34.34, 38.35, 44.18, 44.28, 67.41, 115.98, 122.81, 126.18, 126.86, 129.23, 129.51, 130.06, 130.39, 149.92, 154.84, 155.83, 167.48. HRMS ($C_{19}H_{21}ClN_2O_4$ + Na^+): calculated 399.1088 found 399.1081.

4.7.14. 4-((2-(4-Chlorophenoxy)acetamido)methyl)phenyl diethylcarbamate (14)

White solid, yield 6 %; m.p. = 86–87 °C. Starting from 2-(4-chlorophenoxy)acetic acid (**36**) and 4-(aminomethyl)phenyl diethylcarbamate (**27**), eluent: CH_2Cl_2/MeOH 95:5. ^{1}H NMR (500 MHz, $CDCl_3$) δ: 1.13–1.31 (m, 6H, $CH_2\underline{CH_3}$), 3.30–3.50 (m, 4H, $\underline{CH_2}CH_3$), 4.42–4.60 (m, 4H, 2H $NH\underline{CH_2}CH$ + 2H $O\underline{CH_2}CO$), 6.71–6.91 (m, 3H, 2H aromatics + 1H NH), 7.04–7.14 (m, 2H aromatics), 7.23–7.30 (m, 4H aromatics). ^{13}C NMR (126 MHz, $CDCl_3$) δ: 13.35, 14.22, 41.87, 42.25, 42.59, 67.55, 115.97, 122.14, 127.16, 128.83, 129.67, 134.25, 151.06, 154.12, 155.66, 167.58. HRMS ($C_{20}H_{23}ClN_2O_4$ + Na^+): calculated 413.1239 found 413.1253.

4.7.15. 4-((2-(4-Chlorophenoxy)acetamido)methyl)phenyl dimethylcarbamate (15)

White solid, yield 2 %; m.p. = 122 °C dec. Starting from 2-(4-chlorophenoxy)acetic acid (**36**) and 4-(aminomethyl)phenyl dimethylcarbamate (**28**), eluent: 100 % CH_2Cl_2, 100 % AcOEt. ^{1}H NMR (500 MHz, $CDCl_3$) δ: 3.01 (s, 3H, CH_3), 3.10 (s, 3H, CH_3), 4.50–4.53 (m, 4H, 2H $NH\underline{CH_2}CH$ + 2H $O\underline{CH_2}CO$), 6.76–6.81 (bs, 1H, NH), 6.83–6.86 (m, 2H aromatics), 7.06–7.10 (m, 2H aromatics), 7.25–7.28 (m, 4H aromatics). ^{13}C NMR (126 MHz, $CDCl_3$) δ: 36.43, 36.70, 42.56, 67.55, 115.97, 122.13, 127.16, 128.84, 129.67, 134.38, 151.03, 154.80, 155.66, 167.59. HRMS ($C_{18}H_{19}ClN_2O_4$ + Na^+): calculated 385.0926 found 385.0924.

4.7.16. 4-((2-(4-Chlorophenoxy)acetamido)methyl)phenyl ethyl(methyl) carbamate (16)

White solid, yield 33 %; m.p. = 67–68 °C. Starting from 2-(4-chlorophenoxy)acetic acid (**36**) and 4-(aminomethyl)phenyl ethyl(methyl) carbamate (**29**), eluent: CH_2Cl_2/AcOEt 1:1. ^{1}H NMR (300 MHz, $CDCl_3$) δ: 1.13–1.36 (m, 3H, $CH_2\underline{CH_3}$), 2.91–3.11 (m, 3H, CH_3), 3.33–3.53 (m, 2H, $\underline{CH_2}CH_3$), 4.45–4.57 (m, 4H, 2H $NH\underline{CH_2}CH$ + 2H $O\underline{CH_2}CO$), 6.74–7.94 (m, 3H aromatics), 7.03–7.15 (m, 2H aromatics), 7.23–7.36 (m, 4H, 3H aromatics + 1H NH). ^{13}C NMR (126 MHz, $CDCl_3$) δ: 12.43, 13.20, 42.58, 44.08, 67.55, 115.97, 122.13, 127.17, 128.84, 129.67, 151.05, 155.66, 167.59. HRMS ($C_{19}H_{21}ClN_2O_4$ + Na^+): calculated 399.1082 found 399.1088.

4.7.17. 3-((2-(4-Chlorophenoxy)acetamido)methyl)phenyl dimethylcarbamate (17)

White solid, yield 56 %; m.p. = 104—106 °C. Starting from 2-(4-chlorophenoxy)acetic acid (**36**) and 3-(aminomethyl)phenyl dimethylcarbamate (**31**), eluent: CH_2Cl_2/MeOH 9:1. ^{1}H NMR (300 MHz, $CDCl_3$) δ: 3.00 (s, 3H, CH_3), 3.09 (s, 3H, CH_3), 4.49–4.55 (m, 4H, 2H $NH\underline{CH_2}CH$ + 2H $O\underline{CH_2}CO$), 6.79–6.97 (m, 3H, 2H aromatics + 1H NH), 7.01–7.13 (m, 3H aromatics), 7.23–7.36 (m, 3H aromatics). ^{13}C NMR (126 MHz, $CDCl_3$) δ: 36.44, 36.69, 42.63, 67.54, 116.00, 121.12, 124.53, 127.09, 129.56, 129.64, 139.76, 151.75, 154.75, 155.69, 167.74. HRMS ($C_{18}H_{19}ClN_2O_4$ + Na^+): calculated 385.0926 found 385.0938.

4.7.18. 3-((2-(4-Chlorophenoxy)acetamido)methyl)phenyl ethyl(methyl) carbamate (18)

White solid, yield 18 %; m.p. = 99–101 °C. Starting from 2-(4-chlorophenoxy)acetic acid (**36**) and 3-(aminomethyl)phenyl ethyl (methyl)carbamate (**32**), eluent: CH_2Cl_2/MeOH 95:5, then *n*-hexane/AcOEt 1:1. ^{1}H NMR (300 MHz, $CDCl_3$) δ: 1.14–1.31 (m, 3H, $CH_2\underline{CH_3}$), 2.92–3.09 (m, 3H, CH_3), 3.33–3.52 (m, 2H, $\underline{CH_2}CH_3$), 4.45–4.56 (m, 4H, 2H $NH\underline{CH_2}CH$ + 2H $O\underline{CH_2}CO$), 6.79–6.96 (m, 3H, 2H aromatics + 1H NH), 6.99–7.17 (m, 3H aromatics), 7.22–7.37 (m, 3H aromatics). ^{13}C NMR (126 MHz, $CDCl_3$) δ: 12.44, 13.21, 33.81, 34.23, 42.64, 44.08, 67.54, 116.00, 121.18, 124.50. 127.08, 129.63, 139.04, 151.75, 154.44, 155.70, 167.73.

HRMS ($C_{19}H_{21}ClN_2O_4$ + Na^+): calculated 399.1082 found 399.1067.

4.7.19. 2-((2-(4-Chloro-2-nitrophenoxy)acetamido)methyl)phenyl ethyl (methyl)carbamate (19)

White solid, yield 15 %; m.p. = 102–104 °C. Starting from 2-(4-Chloro-2-nitrophenoxy)acetic acid (**35**) and 2-(aminomethyl)phenyl ethyl(methyl)carbamate (**26**), eluent: *n*-hexane/AcOEt 9:1 then CH_2Cl_2/MeOH 99:1;. ^{1}H NMR (300 MHz, $CDCl_3$) δ: 1.15–1.30 (m, 3H, $CH_2\underline{CH_3}$), 2.95–3.17 (m, 3H, CH_3), 3.33–3.59 (m, 2H, $\underline{CH_2}CH_3$), 4.41–4.67 (m, 4H, 2H $NH\underline{CH_2}CH$ + 2H $O\underline{CH_2}CO$), 6.94–7.02 (m, 1H aromatic), 7.95–7.23 (m, 2H aromatics), 7.26–7.46 (m, 3H, 2H aromatics + 1H NH), 7.48–7.57 (m, 1H aromatic), 7.93–8.01 (m, 1H aromatic). ^{13}C NMR (126 MHz, $CDCl_3$) δ: 12.45, 13.27, 33.88, 34.33, 38.18, 44.22, 68.29, 116.06, 122.72, 125.91, 126.32, 126.94, 128.94, 129.85, 134.79, 139.22, 149.64, 166.07.

HRMS ($C_{19}H_{20}ClN_3O_6$ + Na^+): calculated 444.0938 found 444.0941.

4.7.20. 4-((2-(4-Chloro-2-nitrophenoxy)acetamido)methyl)phenyl diethylcarbamate (20)

White solid, yield 25 %; m.p. = 99–101 °C. Starting from 2-(4-Chloro-2-nitrophenoxy)acetic acid (**35**) and 4-(aminomethyl)phenyl diethylcarbamate (**27**), eluent: 100 % CH_2Cl_2. ^{1}H NMR (300 MHz, $CDCl_3$) δ: 1.11–1.32 (m, 6H, $CH_2\underline{CH_3}$), 3.28–3.50 (m, 4H, $\underline{CH_2}CH_3$), 4.53 (d, J = 6.0 Hz, 2H, $NH\underline{CH_2}CH$), 4.63 (s, 2H, $O\underline{CH_2}CO$), 6.97–7.12 (m, 3H aromatics), 7.28–8.02 (m, 5H, 4H aromatics + 1H NH). ^{13}C NMR (126 MHz, $CDCl_3$) δ: 13.36, 14.22, 41.87, 42.22, 42.62, 68.14, 116.02, 122.08, 126.46, 127.00, 128.71, 134.35, 135.07, 138.98, 149.57, 150.98, 154.08, 166.10. HRMS ($C_{20}H_{22}ClN_3O_6$ + Na^+): calculated 458.1089 found 458.1100.

4.7.21. 4-((2-(4-Chloro-2-nitrophenoxy)acetamido)methyl)phenyl dimethylcarbamate (21)

Yellow solid, yield 2 %; m.p. = 143–144 °C. Starting from 2-(4-Chloro-2-nitrophenoxy)acetic acid (**35**) and 4-(aminomethyl)phenyl dimethylcarbamate (**28**), eluent: CH_2Cl_2/MeOH 99:1; then 100 % AcOEt; then CH_2Cl_2/AcOEt 9:1. ^{1}H NMR (500 MHz, $CDCl_3$) δ: 3.00 (s, 3H, CH_3), 3.09 (s, 3H, CH_3), 4.54 (d, J = 6.0 Hz, 2H, $NH\underline{CH_2}CH$), 4.64 (s, 2H, $O\underline{CH_2}CO$), 6.97–7.13 (m, 3H aromatics), 7.29–8.05 (m, 5H, 4H aromatics + 1H NH). ^{13}C NMR (126 MHz, $CDCl_3$) δ: 36.43, 36.69, 42.62, 68.14, 115.97, 122.07, 126.50, 127.05, 128.75, 134.35, 135.06, 149.56, 150.98, 154.77, 166.07. HRMS ($C_{18}H_{18}ClN_3O_6$ + Na^+): calculated 430.0776 found 430.0758.

4.7.22. 4-((2-(4-Chloro-2-nitrophenoxy)acetamido)methyl)phenyl ethyl (methyl)carbamate (22)

White solid, yield 10 %; m.p. = 97–99 °C. Starting from 2-(4-Chloro-2-nitrophenoxy)acetic acid (**35**) and 4-(aminomethyl)phenyl ethyl (methyl)carbamate (**29**), eluent: 100 % CH_2Cl_2. ^{1}H NMR (300 MHz, $CDCl_3$) δ: 1.12–1.28 (m, 3H, $CH_2\underline{CH_3}$), 2.90–3.11 (m, 3H, CH_3), 3.33–3.55 (m, 2H, $\underline{CH_2}CH_3$), 4.53 (d, J = 6.0 Hz, 2H, $NH\underline{CH_2}CH$), 4.64 (s, 2H, $O\underline{CH_2}CO$), 6.94–7.16 (m, 3H aromatics), 7.28–8.06 (m, 5H, 4H aromatics + 1H NH). ^{13}C NMR (126 MHz, $CDCl_3$) δ: 12.44, 13.20, 33.79, 34.23, 42.60, 44.05, 68.14, 116.03, 122.07, 126.45, 126.99, 128.71, 134.32, 135.07, 149.57, 150.97, 166.12.

HRMS ($C_{19}H_{20}ClN_3O_6 + Na^+$): calculated 444.0933 found 444.0928.

4.7.23. 3-((2-(4-Chloro-2-nitrophenoxy)acetamido)methyl)phenyl dimethylcarbamate (23)

White solid, yield 36 %; m.p. = 108–110 °C. Starting from 2-(4-Chloro-2-nitrophenoxy)acetic acid (**35**) and 3-(aminomethyl)phenyl dimethylcarbamate (**31**), eluent: CH_2Cl_2/MeOH 95:5; then 100 % AcOEt. ^{1}H NMR (300 MHz, $CDCl_3$) δ: 2.99 (s, 3H, CH_3), 3.09 (s, 3H, CH_3), 4.54 (d, J = 6.1 Hz, 2H, NH$\underline{CH_2}$CH), 4.64 (s, 2H, O$\underline{CH_2}$CO), 6.98–7.18 (m, 4H aromatics), 7.28–7.36 (m, 1H aromatic), 7.47 (t, J = 6.1 Hz, 1H, NH), 7.53–7.60 (m, 1H aromatic), 7.97–8.02 (m, 1H aromatic). ^{13}C NMR (126 MHz, $CDCl_3$) δ: 36.44, 36.67, 42.78, 68.17, 116.06, 121.09, 124.41, 126.44, 127.01, 129.50, 135.50, 138.94, 149.56, 151.77, 154.73, 166.24. HRMS ($C_{18}H_{18}ClN_3O_6 + Na^+$): calculated 430.0776 found 430.0784.

4.7.24. 3-((2-(4-Chloro-2-nitrophenoxy)acetamido)methyl)phenyl ethyl (methyl)carbamate (24)

White solid, yield 12 %; m.p. = 84–86 °C. Starting from 2-(4-Chloro-2-nitrophenoxy)acetic acid (**35**) and 3-(aminomethyl)phenyl ethyl (methyl)carbamate (**32**), eluent: CH_2Cl_2/MeOH 9:1; then *n*-hexane/AcOEt 6:4. ^{1}H NMR (300 MHz, $CDCl_3$) δ: 1.19–1.29 (m, 3H, $CH_2\underline{CH_3}$), 2.85–3.13 (m, 3H, CH_3), 3.33–3.53 (m, 2H, $\underline{CH_2}CH_3$), 4.55 (d, J = 6.1 Hz, 2H, NH$\underline{CH_2}$CH), 4.65 (s, 2H, O$\underline{CH_2}$CO), 6.95–7.19 (m, 4H aromatics), 7.28–7.37 (m, 1H aromatic), 7.40–7.52 (m, 1H, NH), 7.53–7.62 (m, 1H aromatic), 7.92–8.09 (m, 1H aromatic). ^{13}C NMR (126 MHz, $CDCl_3$) δ: 12.44, 13.20, 33.79, 34.23, 42.82, 44.07, 68.17, 116.02, 121.14, 124.40, 126.46, 127.03, 129.57, 135.05, 138.86, 139.03 149.55, 151.77, 166.20. HRMS ($C_{19}H_{20}ClN_3O_6 + Na^+$): calculated 444.0933 found 444.0944.

4.8. Biological methods

4.8.1. Inhibition of cholinesterases and monoamine oxidases

All reagents and enzymes (human recombinant AChE and MAOs; BChE from equine serum) were from Sigma-Aldrich, (Milan, Italy). The spectrophotometric Ellman assay (for cholinesterases) and the spectrofluorimetric assay measuring oxidation of kynuramine to 4-hydroxyquinoline (for monoamine oxidases) were used as previously described [48]. Incubations were carried out in 96-well plates (Greiner Bio-One GmbH, Frickenhausen, Germany) in duplicate. For most active compounds (inhibition > 70 %), IC_{50} was determined from seven solutions (ranging from 10^{-5} to 10^{-11} M as the final concentrations) of inhibitor and prepared by diluting a stock DMSO solution 1000 μM with the work buffer. Plate readings were made with Infinite M1000 Pro multiplate reader (Tecan, Cernusco S.N., Italy). Inhibition kinetics for hAChE were investigated using four concentrations of inhibitor (0–40 nM) and six concentrations of substrate acetylthiocholine (from 0.033 to 0.200 mM). IC_{50} values and inhibition values were calculated with the software GraphPad Prism (version 5.01 for Windows; GraphPad Software, San Diego, CA, USA) as the mean of three independent experiments and are expressed as mean ± SEM.

4.8.2. FAAH inhibition

FAAH inhibition assays were performed in triplicate using 96-well black flat-bottom microtiter NBS plates (COSTAR flat black). In a total volume of 200 μL, different concentrations of each potential inhibitor were preincubated in an appropriate fluorometric assay buffer (tris-HCl 125 mM, $Na_2EDTA{\cdot}2H_2O$ 1 mM, pH = 9.0) with the enzyme (FAAH human recombinant, Cayman Chemical, Ann Arbor, MI, USA) for 10 min at room temperature, maintaining the plate in orbital shaking. The substrate (7-amino-4-methyl-2H-1-benzopyran-2-one-5Z,8Z,11Z,14Z-eicosatetraen-amide, AMC-AA, 5 μM final concentration) was then added, and the assay was incubated for 2 h at 37 °C in a TECAN infinite M1000Pro plate reader (Tecan, Männedorf, Switzerland) which read the fluorescence from each well every 30 s (λex = 340 nm, λem = 450 nm), expressing FAAH activity as relative fluorescence units (RFU) [27,49,50]. Percent inhibition for each tested compound were calculated using control wells lacking the inhibitor and blank wells lacking both inhibitor and enzyme. IC_{50} values were calculated using the nonlinear regression function (dose–response inhibition curve) on GraphPad Prism 5.0 (GraphPad Software, La Jolla, CA, USA) and are expressed as mean ± SEM of at least three independent measurements performed in triplicate [27,49,50].

4.8.3. Metal complexation studies

Aqueous $FeCl_3$ (0.0177 M) and $CuCl_2$ (0.015 M) stock solutions were prepared from 1000 ppm Titrisol standards and their metal content was evaluated by flame atomic absorption spectroscopy. Solutions of 0.1 M HCl and 0.1 N KOH (titrant) were prepared from Titrisol ampoules and used for the calibration of the glass electrode. The iron stock solution was prepared in acid excess, to avoid hydrolysis, and its acid content was determined by the standard-addition method using 0.1 N HCl. The titrant (0.1 N KOH) was standardized by titration with potassium hydrogen phthalate solution and discarded when the percentage of carbonate, determined by Gran's method [51], was greater than 0.5 % of the total amount of base. The strong acid–strong base (HCl/KOH) calibrations of the pH electrode were performed with an automated potentiometric apparatus containing a Crison micropH 2002 millivoltimeter, a Crison microBu 2031 burette and a Haake thermostatic bath (T = 25.0 ± 0.1 °C), controlled by PASAT program. The spectrophotometric measurements were done with a Perkin-Elmer Lambda 35 spectrophotometer.

Job plot method was used, with the glass electrode previously conditioned in a 10 % DMSO/water medium. The spectrophotometric measurements were performed in a final volume of 20.00 mL and the ligand (**ROS151**) concentration (C_L) was 8 × 10^{-5} M, under different C_M/C_L ratios (T = 25.0 ± 0.1 °C, ionic strength (I) 0.1 M KCl), by adding adequate volumes of $FeCl_3$ or $CuCl_2$ stock solution and keeping the pH ca 4.0 (Fe^{3+}/L) or 6.0 (Cu^{2+}/L). The same procedure was done for solutions of iron with equal concentrations, in order to correct the absorbance values in the spectra of the Fe^{3+}/**ROS151** system. The chosen wavelength was 303 and 319 nm for the Fe^{3+}/L and Cu^{2+}/L systems, respectively.

4.8.4. In vitro cytotoxycity

The *in vitro* cytotoxicity of compounds **5** (**ROS151**), **6**, **8** and **23** was evaluated by the 3-(4,5-di-methylthiazol-2-yl)-2,5-diphenyltetrazolium bromide (MTT) assay towards a set of 3 human tumor cell lines which includes HepG2 (liver), MCF-7 (breast), and HEK-293 (kidney). Cells were seeded at a density of ≈15000 cells per well into 96-well flat bottom culture plates containing 50 μL of the test compounds (ranged from 30 μM to 300 nM final concentration) in a final volume of 100 μL. Untreated cells were used as positive controls. After 48 h of incubation at 37 °C in a 5 % CO_2 atmosphere, MTT was added to a final concentration of 0.5 mg mL^{-1}. After a further 3–4 h incubation under the same conditions, the culture medium was removed, and the insoluble product was dissolved by the addition of 100 μL of solvent (1:1 v/v DMSO/EtOH). The absorbance of each well was measured at 570 nm using a PerkinElmer Victor V3 plate reader. The 50 % inhibitory concentration (IC_{50}) was defined as the concentration that reduced the absorbance of the untreated wells by 50 % of the vehicle (1 % DMSO) and was determined from dose–response curves using GraphPad PRISM version 5.0. Assays were performed in quadruplicate on three independent experiments. Significant differences in cell viability between treated cells and the solvent control group were analysed using a One-Way Analysis of Variance (ANOVA) and Dunnett's multiple comparison test.

4.8.5. Inhibition of $A\beta_{42}$ aggregation

The inhibitory capacity of the compounds for $A\beta_{42}$ self- aggregation was evaluated by using an already reported method based on the fluorescence emission of thioflavin T [52–54]. Stock solutions of 500 mg ·

L^{-1} of the compounds were prepared in 50 % MeOH/DMSO medium and then working solutions (240 μM) of the hybrids were prepared by adequate dilution of the respective stock solutions with phosphate buffer (0.215 M, pH = 8). $A\beta_{42}$ (Shangai Royobiotech Co., LTD) was pre-treated with 1,1,1,3,3,3-hexafluoro-2-propanol (HFIP), by brief vortexing, and keeping it overnight at room temperature. After partition and solvent evaporation, the $A\beta_{42}$ aliquots were stored at −20 °C. To obtain the $A\beta_{42}$ working solution, the $A\beta_{42}$ aliquots were dissolved with a freshly prepared mixture of 69.5 μL of CH_3CN/Na_2CO_3 (300 μM)/NaOH (250 mM), by brief sonication and vortexing, and then diluted with phosphate buffer to obtain an $A\beta_{42}$ working solution of 40 μM. Solutions in phosphate buffer medium, containing $A\beta_{42}$ (40 μM), in the presence or absence of each ligand (40 μM), were incubated at 37 °C for 24 h. Afterwards, the samples, containing 180 μL of glycine-NaOH 50 mM buffer (pH = 8.50) with 5 μM of ThT, were added to a 96-well microplate (BD Falcon) and fluorescence measurements were monitored in a fluorimeter (microplate reader BMG Labtech, POLARstar OPTIMA) with an excitation wavelength of 445 nm and an emission wavelength of 485 nm. The obtained results are expressed as percentage of inhibition of $A\beta_{42}$ aggregation, through the following equation:

$$\%I = 100(\Delta F_1/\Delta F_0 \times 100)$$

in which ΔF_1 and ΔF_0 are the fluorescence intensities, in the presence and the absence of the tested compound subtracted of the fluorescence intensities due to the respective blanks. The obtained inhibitory values are the mean (SEM < 10 %) of at least three independent experiments performed in duplicate.

5. Pharmacokinetic properties

a) Chemicals and standards solutions

Standard compounds and chemicals for buffer preparation were purchased from Sigma Aldrich (Schnelldorf, Germany) in the highest available purity and from Gall Pharma (Judenburg, Austria) as pharmaceutical standards. Formic acid was ordered from Carl Roth (Karlsruhe, Germany). Solvents for chromatography were purchased from Merck (Darmstadt, Germany) in HPLC or LC-MS grade depending on the analyses. Pooled Sprague Dawley rat plasma (stabilized with K2 EDTA) was purchased from BioTrend (Vienna, Austria) and pooled human plasma from Biowest (Nuaillé, France).

The stock solutions for compounds 23, 8, 6 and ROS151, as well as all standards for the biomimetic chromatography evaluation were prepared at a concentration of 1 mg/mL in DMSO.

The standard mix for the experimental determination of LogP was prepared by dissolving approximately 2 mg of triphenylene and 0.2 mL of toluene in methanol to a final volume of 20 mL. Samples for the HPLC runs were obtained by mixing the stock solution [1 mg/mL] and the standard mix (1:1 v/v).

Sample preparation for the PPB (HSA and AGP) determination consisted of mixing the stock solution with a mixture of 50 mM ammonium acetate buffer (pH adjusted at 7.4) and 2-propanol (1:1 v/v).

Blood-brain barrier penetration assay samples were prepared by mixing the stock solution with a Dulbeccós phosphate-buffered saline containing 20 % acetonitrile (1:1 v/v).

b) Methods

LogP

The samples for Log*P* determination were analyzed on a Shimadzu Prominence LC-20AD XR liquid chromatograph device (Shimadzu Corporation, Tokyo, Japan) equipped with a Shim-pack GIST Column C18 (3 μm, 4.6 × 50 mm, Shimadzu Corporation, Tokyo, Japan). Analyses were performed with a gradient elution of methanol (solvent B) (Merck KGaA, Darmstadt, Germany) and a mixture of 0.01 M phosphate buffer pH 7.4 and methanol (1:1 v/v; solvent A). The gradient was applied as followed: 0 % to 80 % B from minute 0 to 8 min followed by 4 min at 80 % B. The flow rate was at 1.2 mL/min and the column oven was maintained at 40 °C. The injection volume was 10 μL. For the determination of the retention times, the peaks of the references and the test compound were integrated at a wavelength of 254 nm. All measurements were performed in triplicates. The Log*P* values were calculated applying toluene and triphenylene as standards following the protocol of Donovan et al. [55]. For more details see supplementary information [Equation S1].

Plasma protein binding (PPB)

Measurements were performed on a Shimadzu Prominence LC-20AD XR liquid chromatograph device (Shimadzu Corporation, Tokyo, Japan) with the biomimetic chromatography columns CHIRALPAK-HSA (5 μm, 3 × 50 mm, Daicel Inc., Tokyo, Japan) and CHIRALPAK-AGP (5 μm, 3 × 50 mm, Daicel Inc., Tokyo, Japan). For the optimized gradient (0–3 min 0 % B; 3–10 min 30 % B) solvent B was 2-propanol and solvent A 50 mM ammonium acetate buffer adjusted at a pH of 7.4 Flow rate was set at 1.0 mL/min and the column oven was maintained at 30 °C. All measurements were performed in triplicates.

For the calibration of the HSA column 20 standards with known PPB properties were used (see SI). The calibration curve with a R^2 greater than 0.96 was applied to calculate experimental $\%PPB_{HSA}$ as well as estimated %HSA and %AGP by extrapolation following the protocol of Valko et al. [37] applying experimental k_{HSA} and k_{AGP} respectively. Note that these values are obtained with biomimetic stationary phases and refer to binding of the molecule to the specific proteins but do not give the ratio between binding to HSA and AGP in plasma.

Blood-brain barrier penetration (BBB) screening via IAM chromatography

Experiments were conducted on a Nexera XR UHPLC system (Shimadzu Corporation, Tokyo, Japan) with the IAM.PC.DD.2 (100 × 4.6 mm, 10 μm, Regis Technologies, Morton Grove, IL) column. Method described by Yoon et. al. [56] was adapted by changing the flow rate to 1.0 mL/min and the column oven was set at 37 °C. The k_{IAM} of 17 structurally diverse reference standards (molecular weight range between 138.1 and 416.0) was determined. In total 10 of the standards were positive for blood–brain penetration (CNS^+) and seven were negative (CNS^-). For the calculation of the coefficient of membrane permeability (*Pm*) via passive diffusion, the equation 1. with the correction of molecular size to the order of 4 was used.

Equation 1. Formula for the calculation of the coefficient of membrane permeability; k_{IAM} capacity factor on the IAM column; MW-molecular weight:

$P_m = \frac{k_{IAM}}{MW^4} * 10^{10} CNS$ + reference standards had a *Pm* value higher 1.88, while the CNS- reference standards a *Pm* value smaller than 1.55.

Plasma stability

For the plasma stability assessment each compound was prepared in triplicate. The pooled human plasma was pre-warmed with the Eppendorf ThermoMixer comfort (Eppendorf, Austria) at 37 °C for 5 min before mixing with the stock solution. The tubes were incubated for 24 h at 37 °C under gentle shaking. For the termination of the reaction and protein precipitation, 1:2.5 v/v of the ice-cold MeOH containing the IS (donepezil) was added. Samples were centrifuged for 15 min at 14 000 × g at 4 °C. Termination was carried out at 0, 0.5, 1, 1.5, 2, 4 and 24 h, with t_0 at 0 min being the 100 % unmetabolized compound. Measurements were performed on a UHPLC Shimadzu Nexera XR System (Shimadzu Corporation, Tokyo, Japan) equipped with a Kinetex Phenyl-Hexyl column (2.6 μm, 2.1 × 50 mm, Phenomenex, Inc., Torrance, CA, United States) and a precolumn. LC-MS grade water containing 0.1 % formic acid (A) and LC-MS grade methanol containing 0.1 % formic acid (B) were used as mobile phases. The following gradient was applied: 20 % solvent B at 0–1 min, 20–95 % solvent B at 1–7 min, a washing phase at 95 % solvent B from 7 to 10 min. Oven temperature was set to 37 °C, injection volume was 10 μL, and the flow rate maintained at 0.5 mL/min.

6. Docking studies

For each of the examined compounds, starting from the relative SMILES strings, proper ionization was assigned with QUACPAC [57], then a 2D to 3D conversion was achieved with Maestro [58] and thereafter using the Universal Force Field 10,000 steps of Steepest Descent were performed to relax the whole skeleton with Open Babel [59]. X-ray structures for the enzyme-inhibitor complexes of hAChE (chain A; pdb code 6O4W) [38], hBChE (pdb code 7BGC) [39], hFAAH (pdb code 4DO3) [41] and hMAO-B (pdb code 7P4F) [42] were selected for dockings, and checked with the Protein Preparation Wizard interface of Maestro. Electrostatic charges for proteins atoms were loaded according to AMBER UNITED force field [60], while the QUACPAC [57] was used in order to achieve Marsili-Gasteiger charges for the inhibitors and FAD moiety of MAO-B. Affinity maps for each enzyme were first calculated on a 0.375 Å spaced 85 × 85 × 85 $Å^3$ cubic box, having the barycentre on the co-crystallized inhibitors poses, and the binding site available space was tested throughout 1000 runs of Lamarckian Genetic Algorithm (LGA) implemented in AUTODOCK 4.2.6 [61] using the GPU-OpenCL algorithm version [62]. The hydration force field parameters [63] were set in order to explicitly evaluate water molecules contribution in the binding, and the population size and the number of energy evaluation figures were set to 300 and 10000000, respectively. Filtering of the docking poses was achieved by an energy-, similarity- and population-based rule, we called **ESP**, where **E** accounts for the free energy of binding, the energy difference between the selected pose and the relative global minimum and the ligand efficacy, **S** the similarity as scored by the Tanimoto_Combo coefficient according to the shape matching algorithm ROCS [64], **P** is the cluster member population.

Author contributions

L.P. conceived and designed the experiments, R.L., S.S., G.L.S., L.B, M.C., A.C., S.C. carried out the experimental work (R.L., synthesis, L.B., G.L.S., M.C., and A.L. biological assays, A.C. *in silico* studies, S.S. HPLC analyses). L.P., V.T., A.C., F.L., M.A.S., P.T. and J.W. provided reagents/materials/analysis tools. L.P., J.W., S.C., A.C. analyzed the data and participated in the discussion of the obtained results; R.L., S.S., S.C., A. C., J.W. and L.P. wrote the first draft of the paper. L.B., V.T., P.T., M.C., M.A.S., F.L., J.W. and L.P. revised the final draft of the paper. All authors have read and agreed to the published version of the manuscript. All authors have approved the final version of the manuscript.

CRediT authorship contribution statement

Rosalba Leuci: Writing – original draft, Methodology, Investigation, Formal analysis, Data curation. **Stefan Simic:** Investigation, Data curation. **Antonio Carrieri:** Writing – original draft, Visualization, Validation, Software, Methodology, Investigation, Formal analysis, Data curation. **Sílvia Chaves:** Writing – original draft, Visualization, Validation, Software, Methodology, Investigation, Formal analysis, Data curation. **Gabriella La Spada:** Investigation. **Leonardo Brunetti:** Writing – review & editing, Methodology, Investigation, Data curation. **Paolo Tortorella:** Supervision. **Fulvio Loiodice:** Writing – review & editing, Resources, Funding acquisition. **Antonio Laghezza:** Writing – original draft, Visualization, Validation, Software, Methodology, Investigation, Formal analysis, Data curation. **Marco Catto:** Writing – review & editing, Writing – original draft, Supervision, Resources, Methodology, Investigation, Formal analysis, Data curation. **M.Amélia Santos:** Writing – review & editing, Supervision, Resources, Funding acquisition. **Vincenzo Tufarelli:** Supervision, Resources, Funding acquisition. **Judith Wackerlig:** Writing – original draft, Validation, Supervision, Resources, Methodology, Investigation, Funding acquisition, Formal analysis, Data curation. **Luca Piemontese:** Writing – review & editing, Supervision, Resources, Project administration, Funding acquisition, Conceptualization.

Funding

The work was funded by University of Bari Aldo Moro – Fondo ordinario Ricerca scientifica (ex 60 %) 2017–18, by the Portuguese Fundação para a Ciência e Tecnologia (FCT), through project grants UIDB/00100/2020 (https://doi.org/10.54499/UIDB/00100/2020) and UIDP/00100/2020 (https://doi.org/10.54499/UIDP/00100/2020) and finanziato dall'Unione Europea—Next Generation EU Missione 4 Componente 1—CUP: H53D23007940001; PRIN 2022 PNRR, project title: "NInFA" cod. P2022LZBN2 (limited to the synthesis of rivastigmine-like moieties development).

Declaration of competing interest

The authors declare that they have no known competing financial interests or personal relationships that could have appeared to influence the work reported in this paper.

Acknowledgements

Authors would like to thank Vito Bellomo, Anna Scarongella, Giorgia Abbate, Marco Cerini for the technical support in the synthesis of intermediates and/or final compounds, and Paola Settanni and Maria Antonietta Maggio for the technical support in metal chelation and amyloid aggregation studies. This publication is partially based on data collected within the framework of the PhD thesis of Rosalba Leuci.

Appendix A. Supplementary data

Supplementary data to this article can be found online at https://doi.org/10.1016/j.bioorg.2024.107895.

Data availability

Data will be made available on request.

References

[1] L. Piemontese, Historic recurrences in medicinal chemistry: nature-inspired structures as a new opportunity for novel multi-target anti-Alzheimer's drugs, Neural Regen. Res. 18 (12) (2023) 2671–2672, https://doi.org/10.4103/1673-5374.373685.
[2] Alzheimer's Disease Facts and Figures, Alzheimer's & Dementia 19 (4) (2023) 1598–1695, https://doi.org/10.1002/alz.13016.
[3] P. Scheltens, B. De Strooper, M. Kivipelto, H. Holstege, G. Chételat, C.E. Teunissen, J. Cummings, W.M. van der Flier, Alzheimer's Disease, Lancet 397 (10284) (2021) 1577–1590, https://doi.org/10.1016/S0140-6736(20)32205-4.
[4] H. Hampel, M.-M. Mesulam, A.C. Cuello, M.R. Farlow, E. Giacobini, G. T. Grossberg, A.S. Khachaturian, A. Vergallo, E. Cavedo, P.J. Snyder, Z. S. Khachaturian, The cholinergic system in the pathophysiology and treatment of Alzheimer's Disease, Brain 141 (7) (2018) 1917–1933, https://doi.org/10.1093/brain/awy132.
[5] M. Nasb, W. Tao, N. Chen, Alzheimer's Disease Puzzle: Delving into Pathogenesis Hypotheses, Aging Dis. 15 (1) (2024) 43–73. https://doi.org/10.14336/AD.2023.0608.
[6] S. Das, S. Basu, Multi-targeting strategies for Alzheimer's Disease therapeutics: pros and cons, Curr. Top. Med. Chem. 17 (27) (2017) 3017–3061, https://doi.org/10.2174/1568026617666170707130652.
[7] R.T. Bartus, R.L. Dean, B. Beer, A.S. Lippa, The cholinergic hypothesis of geriatric memory dysfunction, Science 217 (4558) (1982) 408–414, https://doi.org/10.1126/science.7046051.
[8] G. Mushtaq, N.H. Greig, J.A. Khan, M.A. Kamal, Status of acetylcholinesterase and butyrylcholinesterase in Alzheimer's Disease and Type 2 diabetes mellitus, CNS Neurol. Disord. Drug Targets 13 (8) (2014) 1432–1439.
[9] S.S. Kaplay, Acetylcholinesterase and butyrylcholinesterase of developing human brain, Biol. Neonat. 28 (1–2) (1976) 65–73, https://doi.org/10.1159/000240805.
[10] B. Li, J.A. Stribley, A. Ticu, W. Xie, L.M. Schopfer, P. Hammond, S. Brimijoin, S. H. Hinrichs, O. Lockridge, Abundant tissue butyrylcholinesterase and its possible function in the acetylcholinesterase knockout mouse, J. Neurochem. 75 (3) (2000) 1320–1331, https://doi.org/10.1046/j.1471-4159.2000.751320.x.
[11] J.R. Atack, E.K. Perry, J.R. Bonham, J.M. Candy, R.H. Perry, Molecular forms of acetylcholinesterase and butyrylcholinesterase in the aged human central nervous system, J. Neurochem. 47 (1) (1986) 263–277, https://doi.org/10.1111/j.1471-4159.1986.tb02858.x.

[12] N.H. Greig, D.K. Lahiri, K. Sambamurti, Butyrylcholinesterase: an important new target in Alzheimer's Disease therapy, Int. Psychogeriatr. 14 (Suppl 1) (2002) 77–91, https://doi.org/10.1017/s1041610203008676.
[13] B. Kumar, Sheetal, A.K. Mantha, V. Kumar, Recent developments on the structure-activity relationship studies of MAO inhibitors and their role in different neurological disorders, RSC Adv. 6 (48) (2016) 42660–42683, https://doi.org/10.1039/C6RA00302H.
[14] J.C. Shih, R.F. Thompson, Monoamine oxidase in neuropsychiatry and behavior, Am. J. Hum. Genet. 65 (3) (1999) 593–598, https://doi.org/10.1086/302562.
[15] T. Behl, D. Kaur, A. Sehgal, S. Singh, N. Sharma, G. Zengin, F.L. Andronie-Cioara, M.M. Toma, S. Bungau, A.G. Bumbu, Role of monoamine oxidase activity in Alzheimer's Disease: an insight into the therapeutic potential of inhibitors, Molecules 26 (12) (2021) 3724, https://doi.org/10.3390/molecules26123724.
[16] R. Leuci, L. Brunetti, A. Laghezza, F. Loiodice, P. Tortorella, L. Piemontese, Importance of biometals as targets in medicinal chemistry: an overview about the role of zinc (II) chelating agents, Appl. Sci. 10 (12) (2020) 4118, https://doi.org/10.3390/app10124118.
[17] R. Leuci, L. Brunetti, V. Tufarelli, M. Cerini, M. Paparella, N. Puvača, L. Piemontese, Role of copper chelating agents: between old applications and new perspectives in neuroscience, Neural Regen. Res. 20 (3) (2025) 751, https://doi.org/10.4103/NRR.NRR-D-24-00140.
[18] L.L. Chen, Y.-G. Fan, L.-X. Zhao, Q. Zhang, Z.-Y. Wang, The metal ion hypothesis of alzheimer's disease and the anti-neuroinflammatory effect of metal chelators, Bioorg. Chem. 131 (2023) 106301, https://doi.org/10.1016/j.bioorg.2022.106301.
[19] L. Brunetti, A. Laghezza, F. Loiodice, P. Tortorella, L. Piemontese, Combining Fatty Acid Amide Hydrolase (FAAH) Inhibition with Peroxisome Proliferator-Activated Receptor (PPAR) activation: a new potential multi-target therapeutic strategy for the treatment of Alzheimer's Disease, Neural Regen. Res. 15 (1) (2020) 67–68, https://doi.org/10.4103/1673-5374.264458.
[20] B.S. Basavarajappa, M. Shivakumar, V. Joshi, S. Subbanna, Endocannabinoid system in neurodegenerative disorders, J. Neurochem. 142 (5) (2017) 624–648, https://doi.org/10.1111/jnc.14098.
[21] T.H. Ferreira-Vieira, I.M. Guimaraes, F.R. Silva, F.M. Ribeiro, Alzheimer's Disease: targeting the cholinergic system, Curr. Neuropharmacol. 14 (1) (2016) 101–115, https://doi.org/10.2174/1570159x13666150716165726.
[22] B. Reisberg, R. Doody, A. Stöffler, F. Schmitt, S. Ferris, H.J. Möbius, Memantine Study Group, Memantine in moderate-to-severe Alzheimer's disease, N. Engl. J. Med. 348 (14) (2003) 1333–1341, https://doi.org/10.1056/NEJMoa013128.
[23] T.B. Ameen, S.N. Kashif, S.M.I. Abbas, K. Babar, S.M.S. Ali, A. Raheem, Unraveling Alzheimer's: The promise of aducanumab, lecanemab, and donanemab, Egypt. J. Neurol. Psychiat. Neurosurg. 60 (1) (2024) 72, https://doi.org/10.1186/s41983-024-00845-5.
[24] M. Revi, Alzheimer's Disease therapeutic approaches, Adv. Exp. Med. Biol. 1195 (2020) 105–116, https://doi.org/10.1007/978-3-030-32633-3_15.
[25] J.W. Wright, J.W. Harding, The Development of Multi-Target-Directed Ligands (MTDL) to Treat Alzheimer's Disease, in: Frontiers in Clinical Drug Research - Alzheimer Disorders, Vol. 1, Bentham Science Publisher, 2013, pp. 86–108.
[26] M.L. Bolognesi, R. Banzi, M. Bartolini, A. Cavalli, A. Tarozzi, V. Andrisano, A. Minarini, M. Rosini, V. Tumiatti, C. Bergamini, R. Fato, G. Lenaz, P. Hrelia, A. Cattaneo, M. Recanatini, C. Melchiorre, Novel class of quinone-bearing polyamines as multi-target-directed ligands to combat Alzheimer's Disease, J. Med. Chem. 50 (20) (2007) 4882–4897, https://doi.org/10.1021/jm070559a.
[27] L. Brunetti, R. Leuci, A. Carrieri, M. Catto, S. Occhineri, G. Vinci, L. Gambacorta, H. Baltrukevich, S. Chaves, A. Laghezza, C.D. Altomare, P. Tortorella, M.A. Santos, F. Loiodice, L. Piemontese, Structure-based design of novel donepezil-like hybrids for a multi-target approach to the therapy of Alzheimer's Disease, Eur. J. Med. Chem. 237 (2022) 114358, https://doi.org/10.1016/j.ejmech.2022.114358.
[28] M.L. Onor, M. Trevisiol, E. Aguglia, Rivastigmine in the treatment of Alzheimer's Disease: an update, Clin. Interv. Aging 2 (1) (2007) 17–32, https://doi.org/10.2147/ciia.2007.2.1.17.
[29] D. Vicente-Zurdo, L. Brunetti, L. Piemontese, B. Guedes, S.M. Cardoso, D. Chavarria, F. Borges, Y. Madrid, S. Chaves, M.A. Santos, Rivastigmine-Benzimidazole hybrids as promising multitarget metal-modulating compounds for potential treatment of neurodegenerative diseases, Int. J. Mol. Sci. 24 (9) (2023) 8312, https://doi.org/10.3390/ijms24098312.
[30] D. Vicente-Zurdo, N. Rosales-Conrado, M.E. León-González, L. Brunetti, L. Piemontese, A.R. Pereira-Santos, S.M. Cardoso, Y. Madrid, S. Chaves, M. A. Santos, Novel rivastigmine derivatives as promising multi-target compounds for potential treatment of Alzheimer's Disease, Biomedicines 10 (7) (2022) 1510, https://doi.org/10.3390/biomedicines10071510.
[31] M.W. Jann, Rivastigmine, a new-generation cholinesterase inhibitor for the treatment of Alzheimer's Disease, Pharmacotherapy 20 (1) (2000) 1–12, https://doi.org/10.1592/phco.20.1.1.34664.
[32] J. Fan, I.A.M. de Lannoy, Pharmacokinetics, Biochem. Pharmacol. 87 (1) (2014) 93–120, https://doi.org/10.1016/j.bcp.2013.09.007.
[33] K.L. Valko, Biomimetic chromatography—a novel application of the chromatographic principles, Analyt. Sci. Adv. 3 (3–4) (2022) 146–153, https://doi.org/10.1002/ansa.202200004.
[34] C. Vraka, L. Nics, K.-H. Wagner, M. Hacker, W. Wadsak, M. Mitterhauser, LogP, a Yesterday's Value? Nucl. Med. Biol. 50 (2017) 1–10, https://doi.org/10.1016/j.nucmedbio.2017.03.003.
[35] B. Seltzer, Donepezil: a review, Expert Opin. Drug Metab. Toxicol. 1 (3) (2005) 527–536, https://doi.org/10.1517/17425255.1.3.527.
[36] N. Kandiah, M.C. Pai, V. Senanarong, I. Looi, E. Ampil, K.W. Park, A.K. Karanam, S. Christopher, Rivastigmine: The advantages of dual inhibition of acetylcholinesterase and butyrylcholinesterase and its role in subcortical vascular dementia and parkinson's disease dementia, in: Clinical Interventions in Aging, vol. 12, Dove Medical Press Ltd, 2017, pp. 697–707, https://doi.org/10.2147/CIA.S129145.
[37] K. Valko, S. Nunhuck, C. Bevan, M.H. Abraham, D.P. Reynolds, Fast gradient HPLC method to determine compounds binding to human serum albumin. Relationships with octanol/water and immobilized artificial membrane lipophilicity, J. Pharm. Sci. 92 (11) (2003) 2236–2248, https://doi.org/10.1002/jps.10494.
[38] O. Gerlits, K.-Y. Ho, X. Cheng, D. Blumenthal, P. Taylor, A. Kovalevsky, Z. Radić, A new crystal form of human acetylcholinesterase for exploratory room-temperature crystallography studies, Chem. Biol. Interact. 309 (2019) 108698, https://doi.org/10.1016/j.cbi.2019.06.011.
[39] M. Rossi, M. Freschi, L. de Camargo Nascente, A. Salerno, S. de Melo Viana Teixeira, F. Nachon, F. Chantegreil, O. Soukup, L. Prchal, M. Malaguti, C. Bergamini, M. Bartolini, C. Angeloni, S. Hrelia, L.A. Soares Romeiro, M. L. Bolognesi, Sustainable drug discovery of multi-target-directed ligands for Alzheimer's Disease, J. Med. Chem. 64 (8) (2021) 4972–4990, https://doi.org/10.1021/acs.jmedchem.1c00048.
[40] A. Carrieri, A. Barbarossa, M. de Candia, F. Samarelli, C.D. Altomare, K. Czarnota-Łydka, J. Handzlik, L. Brunetti, L. Piemontese, F. Limongelli, G. Lentini, A. Carocci, Chiral pyrrolidines as multipotent agents in Alzheimer and neurodegenerative diseases, in press, Bioorg. Med. Chem. 110 (2024) 117829, https://doi.org/10.1016/j.bmc.2024.117829.
[41] L. Bertolacci, E. Romeo, M. Veronesi, P. Magotti, C. Albani, M. Dionisi, C. Lambruschini, R. Scarpelli, A. Cavalli, M. De Vivo, D. Piomelli, G. Garau, A binding site for nonsteroidal anti-inflammatory drugs in fatty acid amide hydrolase, J. Am. Chem. Soc. 135 (1) (2013) 22–25, https://doi.org/10.1021/ja308733u.
[42] F. Ekström, A. Gottinger, N. Forsgren, M. Catto, L.G. Iacovino, L. Pisani, C. Binda, Dual reversible coumarin inhibitors mutually bound to monoamine oxidase B and acetylcholinesterase crystal structures, ACS Med. Chem. Lett. 13 (3) (2022) 499–506, https://doi.org/10.1021/acsmedchemlett.2c00001.
[43] V. Poliseno, S. Chaves, L. Brunetti, F. Loiodice, A. Carrieri, A. Laghezza, P. Tortorella, J.D. Magalhães, S.M. Cardoso, M.A. Santos, L. Piemontese, Derivatives of tenuazonic acid as potential new multi-target anti-Alzheimer's disease agents, Biomolecules 11 (1) (2021) 111, https://doi.org/10.3390/biom11010111.
[44] S. Chaves, A. Hiremathad, D. Tomás, R.S. Keri, L. Piemontese, M.A. Santos, Exploring the chelating capacity of 2-hydroxyphenyl-benzimidazole based hybrids with multi-target ability as Anti-Alzheimer's agents, New J. Chem. 42 (20) (2018) 16503–16515, https://doi.org/10.1039/C8NJ00117K.
[45] J.S. Renny, L.L. Tomasevich, E.H. Tallmadge, D.B. Collum, Method of continuous variations: applications of job plots to the study of molecular associations in organometallic chemistry, Angew. Chem. Int. Ed. Engl. 52 (46) (2013) 11998–12013, https://doi.org/10.1002/anie.201304157.
[46] L. Piemontese, D. Tomás, A. Hiremathad, V. Capriati, E. Candeias, S.M. Cardoso, S. Chaves, M.A. Santos, Donepezil Structure-based hybrids as potential multifunctional anti-Alzheimer's drug candidates, J. Enzyme Inhib. Med. Chem. 33 (1) (2018) 1212–1224, https://doi.org/10.1080/14756366.2018.1491564.
[47] L. Piemontese, G. Vitucci, M. Catto, A. Laghezza, F.M. Perna, M. Rullo, F. Loiodice, V. Capriati, M. Solfrizzo, Natural Scaffolds with multi-target activity for the potential treatment of Alzheimer's Disease, Molecules 23 (9) (2018) 2182, https://doi.org/10.3390/molecules23092182.
[48] M. Paolino, M. de Candia, R. Purgatorio, M. Catto, M. Saletti, A.R. Tondo, O. Nicolotti, A. Cappelli, A. Brizzi, C. Mugnaini, F. Corelli, C.D. Altomare, Investigation on novel e/z 2-benzylideneindan-1-one-based photoswitches with AChE and MAO-B dual inhibitory activity, Molecules 28 (15) (2023) 5857, https://doi.org/10.3390/molecules28155857.
[49] L. Brunetti, A. Carrieri, L. Piemontese, P. Tortorella, F. Loiodice, A. Laghezza, Beyond the canonical endocannabinoid system. A screening of PPAR ligands as FAAH inhibitors, Int. J. Mol. Sci. 21 (19) (2020) 7026, https://doi.org/10.3390/ijms21197026.
[50] A. Carocci, A. Barbarossa, R. Leuci, A. Carrieri, L. Brunetti, A. Laghezza, M. Catto, F. Limongelli, S. Chaves, P. Tortorella, C.D. Altomare, M.A. Santos, F. Loiodice, L. Piemontese, Novel phenothiazine/donepezil-like hybrids endowed with antioxidant activity for a multi-target approach to the therapy of Alzheimer's Disease, Antioxidants 11 (9) (2022) 1631, https://doi.org/10.3390/antiox11091631.
[51] F.J.C. Rossotti, H. Rossotti, Potentiometric titrations using gran plots: a textbook omission, J. Chem. Educ. 42 (7) (1965) 375, https://doi.org/10.1021/ed042p375.
[52] M. Bartolini, C. Bertucci, M.L. Bolognesi, A. Cavalli, C. Melchiorre, V. Andrisano, Insight into the kinetic of amyloid beta (1–42) peptide self-aggregation: elucidation of inhibitors' mechanism of action, Chembiochem 8 (17) (2007) 2152–2161, https://doi.org/10.1002/cbic.200700427.
[53] X. Chao, X. He, Y. Yang, X. Zhou, M. Jin, S. Liu, Z. Cheng, P. Liu, Y. Wang, J. Yu, Y. Tan, Y. Huang, J. Qin, S. Rapposelli, R. Pi, Design, synthesis and pharmacological evaluation of novel tacrine-caffeic acid hybrids as multi-targeted compounds against Alzheimer's Disease, Bioorg. Med. Chem. Lett. 22 (20) (2012) 6498–6502, https://doi.org/10.1016/j.bmcl.2012.08.036.
[54] L. Bon, A. Banaś, I. Dias, I. Melo-Marques, S.M. Cardoso, S. Chaves, M.A. Santos, New multitarget rivastigmine-indole hybrids as potential drug candidates for Alzheimer's Disease, Pharmaceutics 16 (2) (2024) 281, https://doi.org/10.3390/pharmaceutics16020281.
[55] S.F. Donovan, M.C. Pescatore, Method for measuring the logarithm of the octanol-water partition coefficient by using short octadecyl-poly(vinyl alcohol) high-

performance liquid chromatography columns, J. Chromatogr. A 952 (1–2) (2002) 47–61, https://doi.org/10.1016/s0021-9673(02)00064-x.
[56] C.H. Yoon, S.J. Kim, B.S. Shin, K.C. Lee, S.D. Yoo, rapid screening of blood-brain barrier penetration of drugs using the immobilized artificial membrane phosphatidylcholine column chromatography, J. Biomol. Screen. 11 (1) (2006) 13–20, https://doi.org/10.1177/1087057105281656.
[57] QUACPAC 2.1.0.4, OpenEye Scientific Software, Santa Fe, NM, Http://Www.Eyesopen.Com. OpenEye Scientific Software: Santa Fe, NM.
[58] L.L.C. Schrödinger, Schrödinger Release 2021–1, Maestro, New York, NY, Schrödinger, 2021.
[59] N.M. O'Boyle, M. Banck, C.A. James, C. Morley, T. Vandermeersch, G. R. Hutchison, Open babel: an open chemical toolbox, J. Cheminf. 3 (10) (2011) 33, https://doi.org/10.1186/1758-2946-3-33.
[60] C.I. Bayly, K.M. Merz, D.M. Ferguson, W.D. Cornell, T. Fox, J.W. Caldwell, P. A. Kollman, P. Cieplak, I.R. Gould, D.C. Spellmeyer, A second generation force field for the simulation of proteins, nucleic acids, and organic molecules, J. Am. Chem. Soc. 117 (19) (1995) 5179–5197, https://doi.org/10.1021/ja00124a002.
[61] G.M. Morris, D.S. Goodsell, R.S. Halliday, R. Huey, W.E. Hart, R.K. Belew, A. J. Olson, Automated docking using a lamarckian genetic algorithm and an empirical binding free energy function, J. Comput. Chem. 19 (14) (1998) 1639–1662, https://doi.org/10.1002/(SICI)1096-987X(19981115)19:14<1639::AID-JCC10>3.0.CO;2-B.
[62] L. El Khoury, D. Santos-Martins, S. Sasmal, J. Eberhardt, G. Bianco, F.A. Ambrosio, L. Solis-Vasquez, A. Koch, S. Forli, D.L. Mobley, Comparison of Affinity ranking using autodock-GPU and MM-GBSA scores for BACE-1 inhibitors in the D3R grand challenge 4, J. Comput. Aided Mol. Des. 33 (12) (2019) 1011–1020, https://doi.org/10.1007/s10822-019-00240-w.
[63] S. Forli, A.J. Olson, A force field with discrete displaceable waters and desolvation entropy for hydrated ligand docking, J. Med. Chem. 55 (2) (2012) 623–638, https://doi.org/10.1021/jm2005145.
[64] OpenEye Scientific Software. ROCS, 3.4.0.4, OpenEye Scientific Software, Santa Fe, NM, Hhtp://Www.Eyesopen.Com. Santa Fe, NM.